Systems), and an anti–HOCl–ox-LDL polyclonal antibody (Calbiochem). The recombinant human LOX-1 extracellular domain and a neutralizing anti-mouse LOX-1 monoclonal antibody (TS58) were prepared as described previously (22,23).

Subjects. Ethics approval for this entire study was granted by our institution's Ethics Committee, and written consent was obtained from each patient. In analyses of patients who had received only nonbiologic treatments, patients with a diagnosis of RA (n = 47) according to the American College of Rheumatology revised criteria (24) and patients with OA (n = 32) were studied. Most patients with RA had received methotrexate, and none of the patients had received a biologic agent. Healthy control subjects (n = 30) were individuals who did not meet the classification criteria for RA or any other inflammatory disease (details available from the corresponding author upon request).

In analyses of patients who had received biologic treatments, patients with RA who had no previous exposure to a biologic agent (n = 11) were studied. All of these patients had active disease, defined as a Disease Activity Score in 28 joints (DAS28) of ≥3.2 (25). Blood samples were obtained before and 6 weeks after the beginning of the biologic treatment. In each patient, the biologic agent administered (TNFα soluble receptor [etanercept], antibodies [either infliximab or adalimumab], or IL-6 receptor antibody [tocilizumab]) was chosen at the discretion of the physician. Patients' responses to the treatment were recorded, and the DAS28 was calculated at every visit (details available from the corresponding author upon request).

Preparation of blood, synovial fluid, and synovial tissue samples. Peripheral blood and synovial fluid samples were obtained from the patients with RA and patients with OA. Blood samples were collected in tubes containing ethylenediaminetetraacetic acid dipotassium salt, to separate the plasma. The samples were centrifuged at 400*g* for 7 minutes and stored at −20°C until analyzed. Plasma was isolated from the blood at 1 hour after the blood withdrawal, to avoid the possibility of a change in sLOX-1 by the time of isolation. Synovial tissue samples were obtained from patients with RA undergoing knee joint surgery.

Chemiluminescence enzyme-linked immunoassay (CLEIA). Circulating sLOX-1 levels in the plasma and synovial fluid were measured as previously described (26). Briefly, sLOX-1 levels were measured by a sandwich CLEIA using 2 different human LOX-1–specific monoclonal antibodies, one of which was labeled with a chemiluminescent agent, and recombinant human LOX-1 extracelluar domain as an assay standard. JMP software version 7.01 (SAS Institute) was used to calculate receiver-operating characteristic (ROC) curve values and cutoff points for positivity.

Preparation of LDL and ox-LDL. Human LDL (density 1.019–1.063) was isolated from fresh plasma by ultracentrifugation, as described previously (11). LDL was oxidized at a protein concentration of 3 mg/ml by exposure to 7.5 m*M* $CuSO_4$, and in every preparation, lipopolysaccharide contamination was ruled out. DiI-labeled ox-LDL was prepared according to the manufacturer's instructions (Molecular Probes).

Preparation of conditioned medium. Chinese hamster ovary K1 (CHO-K1) cells stably expressing bovine LOX-1 (BLOX-1–CHO) were cultured in F-12 medium (Sigma-Aldrich) containing 10% fetal bovine serum supplemented with 10 mg/ml of blasticidin S (Funakoshi), as described previously (11). After 48 hours in culture, the cells were washed with phosphate buffered saline (PBS) and subsequently cultured with serum-free F-12 medium for 24 hours. After incubation, the supernatants were pooled for use as conditioned medium (referred to as sLOX-1 original conditioned medium). Alternatively, the supernatants were concentrated using an Amicon Ultra-4 centrifugal filter device (Millipore), and this was used as sLOX-1 concentrated conditioned medium, containing abundant sLOX-1 as a fractionated concentrate (10–50 kd).

DiI-labeled ox-LDL uptake assay. FLS from the knee joint synovium of patients with RA were incubated with serum-free medium for 24 hours. DiI-labeled ox-LDL (20 μg/ml) or medium alone was added to each well, followed by incubation for 24 hours. To exclude nonspecific binding, unlabeled ox-LDL (100 μg/ml) was added to some wells simultaneously with the DiI-labeled ox-LDL. In other wells, an original conditioned medium of BLOX-1–CHO cells containing sLOX-1 was added in combination with DiI-labeled ox-LDL. After a 24-hour incubation period, the RA FLS were washed and fixed in 4% paraformaldehyde/PBS for 10 minutes at room temperature, and after washing, the FLS were counterstained using a SYBR Green I DNA staining system (Molecular Probes). Uptake of the DiI-labeled ox-LDL in these cells was visualized using confocal microscopy (Olympus).

Assessment of experimental knee joint inflammation in vivo. C57BL/6 mice (all 10-week-old males) were used to assess knee joint inflammation. The skin of the mice was incised longitudinally on the center of the right knee joint, and the capsule and patellar tendon were exposed. The mice in the experimental group were subjected to intraarticular injections (10 μl once daily for 7 days) of ox-LDL (2 mg/ml), native LDL (2 mg/ml), or PBS into the right knee joint. One hour before the ox-LDL injection, a group of mice received an intraarticular injection (20 μl once daily for 7 days) of anti–LOX-1 antibody (10 μg/ml), human recombinant LOX-1 protein (1.0 mg/ml), or control IgG (10 μg/ml). After the ox-LDL injection, the incised skin was sutured, and the mice were returned to their cages. All mice were killed 24 hours after the last injection, and the knee joints were harvested. All animal studies were conducted in accordance with principles and procedures approved by the Kyoto University Committee of Animal Resources.

Histologic analysis. Knee joint specimens from the mice were processed as paraffin-embedded sections, with a thickness of 7 μm, and stained with hematoxylin and eosin and Safranin O–fast green. For immunohistochemical analyses, deparaffinized sections were blocked with 0.3% hydrogen peroxide in methanol for 20 minutes. An anti–LOX-1 antibody, an anti–ox-LDL antibody, an anti–MMP-3 antibody, or control IgG was applied to the specimens, followed by incubation for 60 minutes at room temperature. The reaction products were visualized using a Vectastain ABC Kit and a DAB Peroxidase Substrate Kit (Vector) according to the manufacturer's instructions. The severity of joint inflammation was scored on a scale of 0–4, based on the degree of cellular infiltration into the joint tissue and the extent of pannus formation (27). In addition, proteoglycan depletion was scored on an arbitrary scale of 0–4 (28). Joint inflammation and proteoglycan depletion in each section were scored in a

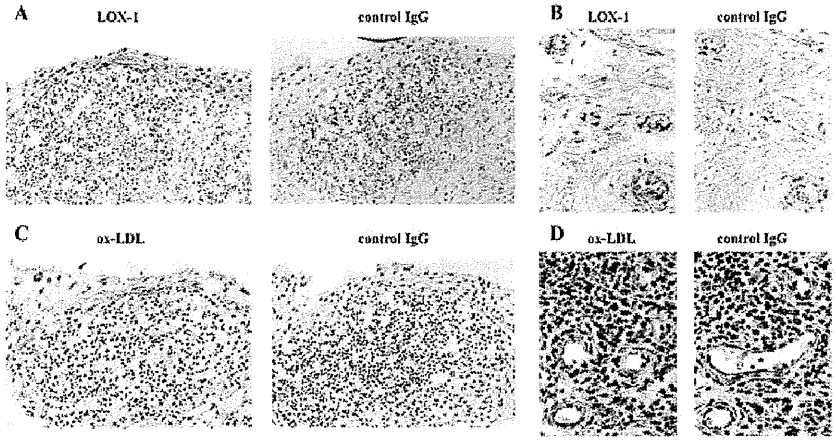

Figure 1. Expression of lectin-like oxidized low-density lipoprotein (ox-LDL) receptor 1 (LOX-1) and ox-LDL in inflamed synovium from a patient with rheumatoid arthritis. Immunohistochemical staining of a representative RA synovial tissue sample for LOX-1 (**A** and **B**) and ox-LDL (**C** and **D**) demonstrates the expression of LOX-1 and ox-LDL in the lining layer (**A** and **C**) and around blood vessels (**B** and **D**). Nonimmune IgG was used as a negative control. Original magnification × 40 in **A** and **C**; × 200 in **B** and **D**.

blinded manner by 2 independent observers (HS and TK), to obtain the mean scores for each measure.

Statistical analysis. Data are presented as the mean ± SEM. Statistical comparisons between 2 groups were per-

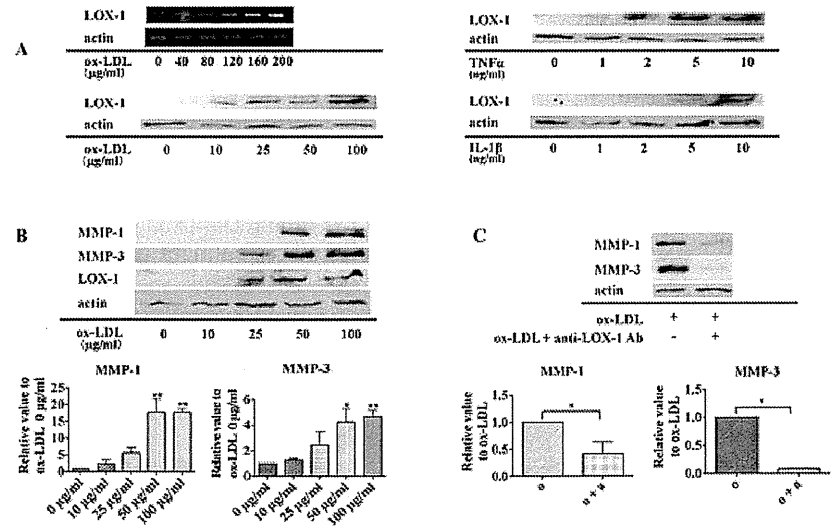

Figure 2. Induction of matrix metalloproteinase 1 (MMP-1) and MMP-3 production by lectin-like oxidized low-density lipoprotein (ox-LDL) receptor 1 (LOX-1) in fibroblast-like synoviocytes (FLS) from patients with rheumatoid arthritis (RA). **A** and **B**, RA FLS were stimulated with the indicated concentrations of ox-LDL, tumor necrosis factor α (TNFα), or interleukin-1β (IL-1β) for 24 hours. Total RNA was assessed by reverse transcription–polymerase chain reaction (**A** [top left]), and supernatants were assessed by immunoblotting (**A** [bottom left, top and bottom right] and **B** [top]), to determine the expression of LOX-1 (**A**) and MMPs 1 and 3 (**B**); β-actin was used as a positive control. The cumulative data derived from immunoblotting were assessed semiquantitatively in densitometric analyses, with results expressed as the mean ± SEM levels of MMPs 1 and 3 after stimulation with the various concentrations of ox-LDL, relative to the values without stimulation (0 μg/ml ox-LDL) (**B** [bottom]). * = $P < 0.05$; ** = $P < 0.01$, versus cultures without stimulation. **C**, RA FLS were incubated with anti–LOX-1 antibody (Ab) (10 μg/ml) (a) for 1 hour before exposure to ox-LDL (100 μg/ml) (o) for 24 hours. Cells were then lysed and subjected to immunoblotting to detect protein levels of MMPs 1 and 3 (top). The cumulative data derived from immunoblotting were assessed semiquantitatively in densitometric analyses, with results expressed as the mean ± SEM levels of MMPs 1 and 3 in cultures with ox-LDL plus antibody relative to cultures with ox-LDL alone (bottom). * = $P < 0.05$. The data in **B** and **C** are representative of at least 4 independent experiments.

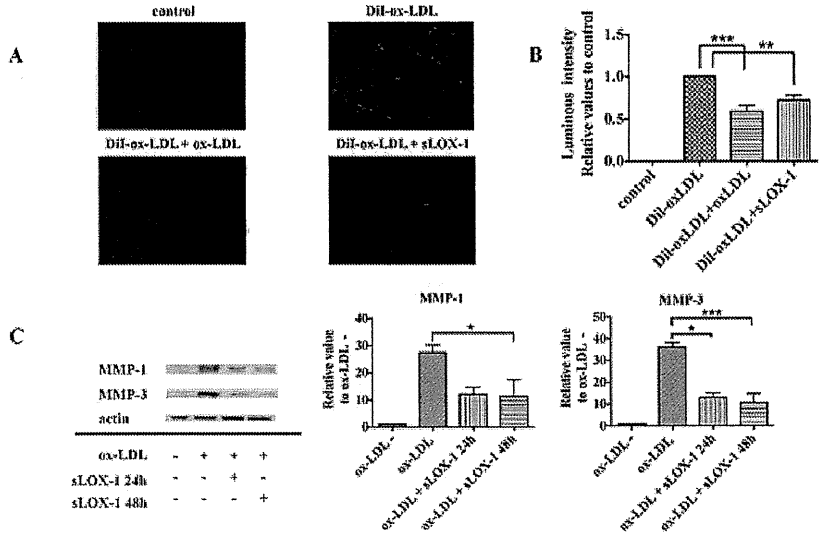

Figure 3. Uptake of DiI-labeled oxidized low-density lipoprotein (ox-LDL) into rheumatoid arthritis (RA) fibroblast-like synoviocytes (FLS), and decrease in the ox-LDL–induced production of matrix metalloproteinase 1 (MMP-1) and MMP-3 in RA FLS by soluble lectin-like ox-LDL receptor 1 (sLOX-1). **A,** RA FLS were treated with medium alone (control), 20 μg/ml of DiI-labeled ox-LDL (top right), DiI-labeled ox-LDL in the presence of an excess amount of unlabeled ox-LDL (100 μg/ml) (bottom left), or DiI-labeled ox-LDL in combination with an original conditioned medium containing sLOX-1 (100 μg/ml) (bottom right). Representative results are shown. Original magnification × 200. **B,** The relative fluorescence intensities of DiI labeling of ox-LDL uptake were measured in RA FLS treated with DiI-labeled ox-LDL alone, excess unlabeled ox-LDL, or excess sLOX-1, with results expressed as the mean ± SEM of 4 samples per group, relative to that in medium alone (control). ** = $P < 0.01$; *** = $P < 0.001$. **C,** Protein levels of MMP-1 and MMP-3 were determined in the supernatants after RA FLS were treated with an sLOX-1 concentrated conditioned medium that contained abundant sLOX-1 (100 μg/ml), in the absence or presence of ox-LDL, for 24 or 48 hours. Results were assessed by immunoblotting (left) and expressed as the mean ± SEM protein levels in 4 samples per group, relative to that in cultures without ox-LDL (ox-LDL−) (middle and right). * = $P < 0.05$; *** = $P < 0.001$.

formed using a Student's 2-tailed t-test. Differences among 3 groups were analyzed using the Bonferroni method. Relationships between sLOX-1 and other variables were evaluated using Pearson's correlation analyses. Differences were considered significant when P values were less than 0.05.

RESULTS

Abundant accumulation of ox-LDL and enhanced expression of LOX-1 protein in the synovial tissue of RA patients. We first assessed the expression of ox-LDL and LOX-1 proteins in human synovial tissue, the major site of RA inflammation. LOX-1 (Figures 1A and B) and ox-LDL (Figures 1C and D) proteins were clearly identified in the RA synovium, particularly in the lining layer (Figures 1A and C) and around blood vessels (Figures 1B and D), similar to the previously reported localization of MMP-1 and MMP-3 (29).

In addition, treatments with ox-LDL, TNFα, and IL-1β dose-dependently up-regulated the expression of LOX-1 messenger RNA and protein production from FLS in cultures of RA synovium (Figure 2A). Furthermore, incubation of RA FLS with ox-LDL (0–100 μg/ml) for 24 hours increased the production of MMP-1 and MMP-3 proteins in a dose-dependent manner (Figure 2B). Pretreatment of the FLS with the anti–LOX-1 antibody (10 μg/ml) significantly reduced the ox-LDL–stimulated production of MMP-1 and MMP-3 (Figure 2C). Pretreatment with native (nonoxidized) LDL or the anti–LOX-1 antibody alone had no effect on the basal production level of MMP-1 or MMP-3 (results not shown).

Inhibition of ox-LDL–induced production of MMPs 1 and 3 by sLOX-1 concentrated medium. To determine whether sLOX-1 inhibits the ox-LDL–LOX-1 interaction, we first examined the ability of sLOX-1 to inhibit the uptake of DiI-labeled ox-LDL in RA FLS. Incubation of the FLS with DiI-labeled ox-LDL (20 μg/ml) for 24 hours led to the detection of DiI inside the cells (Figure 3A). This uptake was found to be specific, as it was displaced by an excess amount of unlabeled ox-LDL (100 μg/ml). Subsequently, a conditioned medium containing sLOX-1 was added, in combination with the DiI-labeled ox-LDL, and incubated with the FLS for 24 hours. The uptake of ox-LDL was signifi-

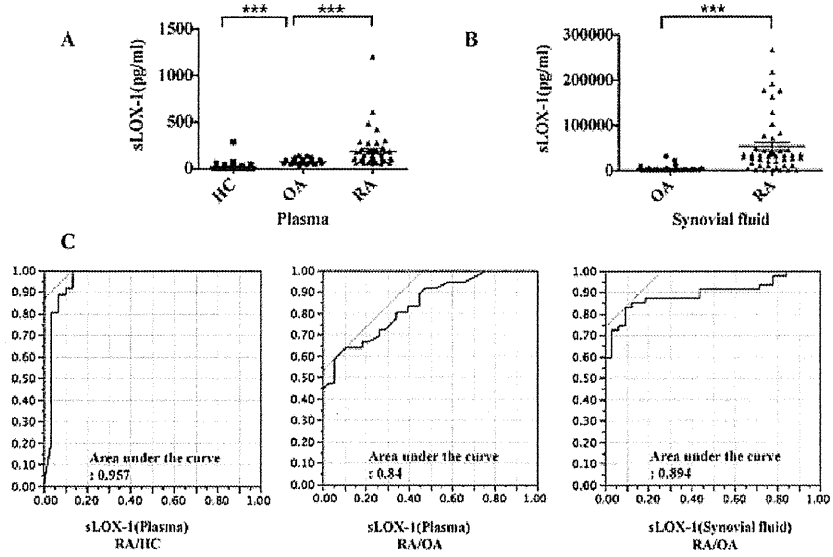

Figure 4. Comparisons of plasma and synovial fluid levels of soluble lectin-like oxidized low-density lipoprotein receptor 1 (sLOX-1) among patients with rheumatoid arthritis (RA), patients with osteoarthritis (OA), and healthy control subjects (HC). **A** and **B**, A marked increase in sLOX-1 levels was found in the plasma (**A**) and synovial fluid (**B**) of RA patients, as compared with OA patients and healthy controls. Bars show the mean ± SEM of samples from individual RA patients, OA patients, and healthy controls. *** = $P < 0.001$. **C**, Receiver operating characteristic curve analyses of the sLOX-1 levels in the plasma or synovial fluid demonstrate that the area under the curve can differentiate patients with RA from patients with OA and healthy controls. These results show that the levels of sLOX-1 in the plasma (left and middle) and in the synovial fluid (right) are a highly sensitive and specific diagnostic marker for RA.

cantly decreased by the sLOX-1 original conditioned medium (Figure 3A). Moreover, as shown in Figure 3B, the inhibitory effect of an excess amount of unlabeled ox-LDL or sLOX-1, compared to that of DiI-labeled ox-LDL alone, was significant.

To further investigate the role of sLOX-1 in mediating the effects of ox-LDL in RA FLS, we tested the effects of sLOX-1 on the expression of MMPs 1 and 3 in the presence of the sLOX-1 concentrated medium. Incubation of the FLS with the sLOX-1 concentrated medium for 24 or 48 hours caused a significant decrease in the ox-LDL–induced production of both MMP-1 and MMP-3 (Figure 3C).

Role of plasma and synovial fluid sLOX-1 as a potent diagnostic marker for RA. To examine whether sLOX-1 is useful for the diagnosis of RA, we analyzed sLOX-1 levels in plasma and synovial fluid from 47 patients with RA (mean age 59 years, age range 17–87 years), 32 patients with OA (mean age 72.1 years, age range 44–80 years), and 30 healthy control subjects (plasma only; mean age 46.5 years, age range 32–60 years). As shown in Figure 4A, sLOX-1 levels in the plasma of RA patients (mean ± SEM 189.3 ± 36 pg/ml) were significantly higher ($P < 0.001$) compared with those in the plasma of OA patients (74.2 ± 3.9 pg/ml) and healthy controls (21.4 ± 9.9 pg/ml). Similarly, in the synovial fluid, the levels of sLOX-1 were significantly higher in the RA group (mean ± SEM 53,548 ± 8,186 pg/ml) than in the OA group (3,893 ± 1,162 pg/ml; $P < 0.001$) (Figure 4B). No correlation between age and sLOX-1 concentration was found (results not shown).

To assess the diagnostic value of the plasma sLOX-1 level, an ROC curve analysis of sLOX-1 was performed (Figure 4C). ROC curve analyses of sLOX-1 plasma levels revealed a high sensitivity and specificity for differentiating patients with RA from healthy controls (area under the curve [AUC] 0.96, at an optimal cutoff point of 57 pg/ml). In ROC curve analyses of sLOX-1 plasma levels comparing RA patients with OA patients, the AUC was 0.84 (at an optimal cutoff point of 99 pg/ml). Similar AUC values were obtained in comparisons of the sLOX-1 levels in the synovial fluid. ROC curve analyses showed that the sLOX-1 levels in the synovial fluid had a higher sensitivity and specificity for differentiating patients with RA from patients with OA (AUC 0.89, at an optimal cutoff point of 11,145.7 pg/ml).

Plasma and synovial fluid sLOX-1 levels as a marker of RA disease activity. To investigate whether the plasma and synovial fluid sLOX-1 levels could reflect

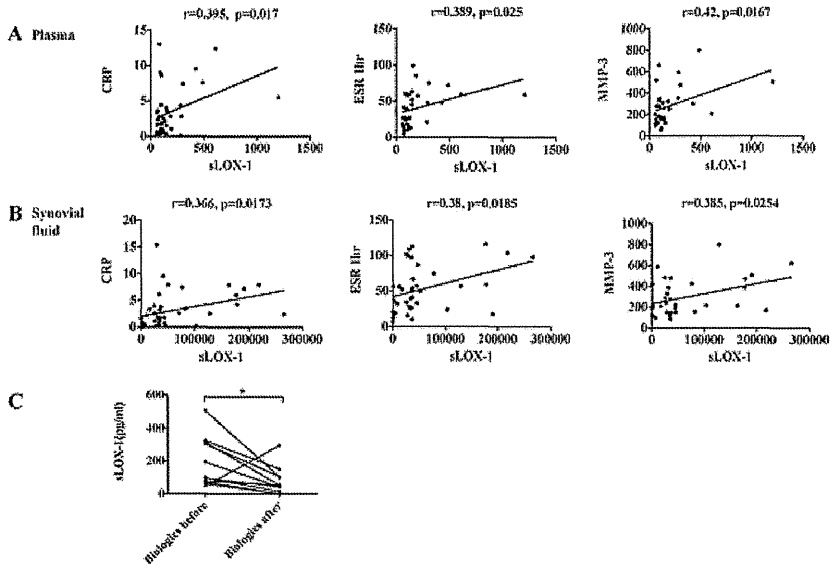

Figure 5. Correlation between the levels of soluble lectin-like oxidized low-density lipoprotein receptor 1 (sLOX-1) and rheumatoid arthritis (RA) biomarkers, such as the C-reactive protein (CRP) level, erythrocyte sedimentation rate (ESR), and matrix metalloproteinase 3 (MMP-3) level, in plasma and synovial fluid samples from patients with RA. **A** and **B,** Circulating sLOX-1 levels in the plasma (**A**) and synovial fluid (**B**) were positively correlated with the CRP level, ESR, and MMP-3 level. **C,** The plasma sLOX-1 levels were examined before and after treatment of RA patients with biologic agents. Plasma sLOX-1 levels were significantly decreased after biologic treatment in all but 1 patient. Representative results from individual patients are shown. * = $P < 0.05$.

the extent of RA disease activity, we examined the correlation between sLOX-1 levels and other clinical laboratory variables. The levels of sLOX-1 in the plasma (Figure 5A) and in the synovial fluid (Figure 5B) correlated with the serum levels of CRP, the ESR, and the levels of MMP-3, but not with the serum levels of LDL cholesterol or other lipoprotein-related markers (results not shown).

To investigate whether sLOX-1 levels in the plasma were decreased by effective biologic treatment, we examined the sLOX-1 levels before and after anticytokine treatment among 11 RA patients who had not previously been treated with a biologic agent. Almost all of the anticytokine therapies decreased the sLOX-1 concentration, irrespective of the agent administered (Figure 5C), and these effects correlated with decreases in the DAS28 (mean ± SEM change from 5.98 ± 0.21 before treatment to 3.19 ± 0.38 after treatment), the serum CRP level (from 3.33 ± 0.50 mg/dl before treatment to 0.33 ± 0.13 mg/dl after treatment), the ESR (from 52.4 ± 4.7 mm/hour before treatment to 15.7 ± 3.8 mm/hour after treatment), and the MMP-3 level (from 429.2 ± 67.4 ng/ml before treatment to 132.1 ± 39.0 ng/ml after treatment) (results not shown).

Improvement in articular cartilage degradation and arthritic changes in ox-LDL–treated mice after blockade of LOX-1. To assess the role of ox-LDL and LOX-1 in the pathogenesis of arthritis in vivo, we injected ox-LDL, native LDL, or PBS into the right knee joints of mice once per day for 7 days and evaluated the development of joint inflammation. The contralateral knees received a sham operation, with a skin incision but no injection. Injection of the materials did not cause any systemic effects, such as weight loss, or apparent morbidities (results not shown).

Differences in knee joint diameters between the injected knee and the contralateral sham-operated knee were substantially increased by the injection of ox-LDL into the right knee joint, whereas differences between the injected knee and the contralateral knee were less substantial when the right knee joint was injected with native LDL (results not shown). Results of immunohistochemistry showed prominent LOX-1 expression in the cartilage and synovium in the ox-LDL–treated group, whereas the native LDL–treated group displayed hardly any positive staining for LOX-1 (results not shown).

To examine whether anti–LOX-1 treatment had any therapeutic efficacy, we administered an anti–

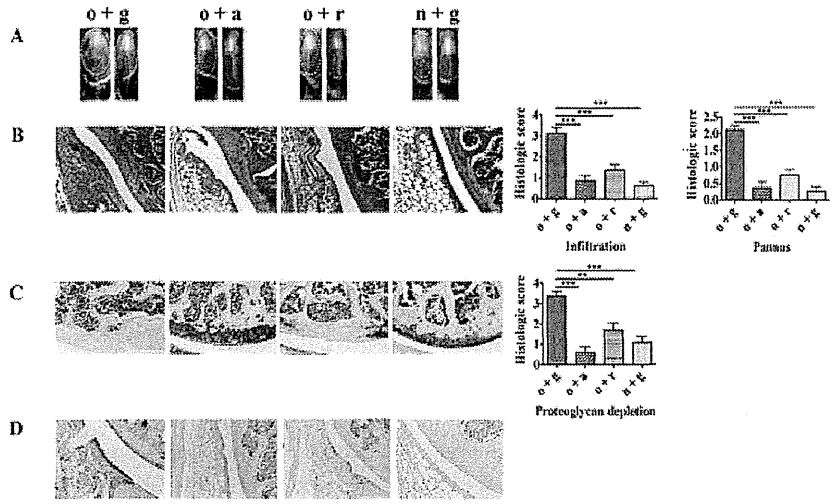

Figure 6. Effects of recombinant soluble lectin-like oxidized low-density lipoprotein (ox-LDL) receptor 1 (sLOX-1) extracellular domain and of an anti–LOX-1 neutralizing antibody on ox-LDL–induced arthritic changes in the knee joints of mice in vivo. **A,** To induce inflammatory arthritis, the right knee joints of mice received an intraarticular injection of ox-LDL (o), or native LDL (n) as a control (left panels in each pair); the contralateral knees received a sham operation (right panels in each pair). One hour prior to injection, the right knee joints were treated with anti–LOX-1 (o + a) or recombinant LOX-1 protein (o + r); IgG was used as a treatment control (o + g or n + g). Representative macroscopic images of paired knee joints from different mice are shown. **B,** Histologic features of joint inflammation (left) and histologic scores for inflammatory cell infiltration and pannus formation (right) were assessed in hematoxylin and eosin–stained, paraffin-embedded knee joint sections in each treatment group (corresponding to the groups shown in **A**). **C,** Histologic features of the cartilage (left) and histologic scores for proteoglycan depletion (right) were assessed in Safranin O–fast green–stained, paraffin-embedded knee joint sections in each treatment group (corresponding to the groups shown in **A**). Results in **B** and **C** are the mean ± SEM of 5 mice per group. ** = $P < 0.01$; *** = $P < 0.001$. **D,** Expression of matrix metalloproteinase 3 (MMP-3) protein was determined using immunohistochemical analyses of the knee joint sections from each treatment group (corresponding to the groups shown in **A**). Original magnification × 200 in **B–D.**

LOX-1 neutralizing antibody, recombinant LOX-1 protein (equivalent to sLOX-1), or control IgG via intraarticular injection 1 hour before ox-LDL administration. Pretreatment with the anti–LOX-1 antibody or recombinant LOX-1 suppressed joint swelling, whereas control IgG did not (Figure 6A). Hematoxylin and eosin staining also revealed that treatment with ox-LDL caused massive synovial hyperplasia, with significantly increased inflammatory cell infiltration and pannus formation, compared with that in the native LDL–treated controls (Figure 6B). In contrast, pretreatment with the anti–LOX-1 antibody or with the recombinant LOX-1 significantly inhibited the synovial hyperplasia induced by ox-LDL treatment, reducing it to the levels observed in the native LDL–treated controls.

In addition, we analyzed the extent of proteoglycan depletion in the mouse joints, using Safranin O staining. The results showed significantly higher depletion in the ox-LDL–treated joints compared with those treated with native LDL (Figure 6C). In contrast, pretreatment with the anti–LOX-1 antibody or the recombinant LOX-1 significantly prevented proteoglycan loss in the articular cartilage.

To clarify the involvement of proteinases in the loss of proteoglycans, the expression of MMP-3 was examined in the mouse joints using immunohistochemical analysis (Figure 6D). High levels of MMP-3 protein were observed in the synovium and articular cartilage after administration of ox-LDL plus control IgG. In contrast, MMP-3 protein expression was markedly reduced in the joints pretreated with the anti–LOX-1 antibody or recombinant LOX-1.

DISCUSSION

The importance of early diagnosis and intervention to prevent the progression of joint damage is well recognized in RA, considering the high propensity of the disease toward joint destruction, even during periods of clinical remission (30). Laboratory tests are critical for the identification of RA at an early stage, as exemplified by the fact that the newly developed RA classification criteria include both diagnostic markers and inflammation markers, in addition to physical findings (31). Recently, we and others have reported that the circulating level of sLOX-1 is a potential diagnostic and prog-

nostic biomarker for acute coronary syndrome (19–21) and is associated with levels of inflammation markers (32).

Consistent with these findings from previous studies, we showed here that sLOX-1 levels in the plasma and synovial fluid of RA patients were markedly elevated as compared with those in non-RA controls. Furthermore, the ROC curve analyses indicated that the diagnostic sensitivity and specificity of sLOX-1 levels for RA were much higher than those obtained when using anti–cyclic citrullinated peptide antibody levels for the diagnosis of RA (33). These results clearly indicate that sLOX-1 is a powerful biomarker to differentiate patients with RA from patients with OA and healthy controls.

Among the currently available clinical tests for the evaluation of RA disease activity, the DAS28 (which includes the CRP level or ESR) is the most widely used in clinical practice. Although the CRP level and ESR are frequently used in the monitoring of patients, these measures are nonspecific for RA and were only weakly correlated with the other parameters of disease activity (34). The present study showed that sLOX-1 levels were positively correlated not only with laboratory markers, such as the CRP level, ESR, and MMP-3 level, but also with the extent of disease activity. A variety of cell types contribute to the increase in sLOX-1 levels in the plasma and synovial fluid, including endothelial cells, articular chondrocytes, and, more importantly, synovial fibroblasts, as well as cells involved in the activation of the immune system in response to various cytokines and ox-LDL. These findings suggest that the production of sLOX-1 is reflective of a whole set of inflammation mechanisms that may contribute to the pathogenesis of RA, and therefore, that sLOX-1 may be a sufficiently reliable biomarker for RA disease activity (Figure 4).

Although previous studies have demonstrated the potential roles of sLOX-1 in atherosclerotic diseases (19–21), the functional role of sLOX-1 in the pathogenesis of RA is not fully understood. We previously reported that ox-LDL was taken up by rat chondrocytes and reduced the viability of the cells via LOX-1 (35). Similarly, in the present study, we demonstrated that ox-LDL was taken up by human RA FLS, thus reducing the viability of the cells (results not shown), and also showed that the addition of sLOX-1 concentrated medium into the cultures significantly decreased the effects of ox-LDL on the production of MMPs 1 and 3 in FLS in vitro (Figure 3C). Consistent with this observation, we demonstrated that the knee joint arthritis induced by ox-LDL injection was decreased in mice treated with recombinant LOX-1 extracellular domain (sLOX-1) in vivo (Figure 6).

Taken together, these results indicate that sLOX-1 may compete with LOX-1 for the uptake of ox-LDL at the cell surface and neutralize inflammation to reduce joint destruction. Therefore, our current results collectively suggest that sufficient pharmacologic amounts of sLOX-1 can competitively prevent ox-LDL from binding to cell surface LOX-1 and reduce the detrimental effects of ox-LDL–LOX-1 signaling. These mechanisms may present an attractive avenue for the development of a desired novel treatment for RA using sLOX-1.

FLS and macrophages are 2 of the predominant cell types involved in RA synovitis. Both types of cells produce high levels of proinflammatory cytokines and mediate inflammatory cell responses in RA. Studies have shown that LOX-1 is expressed by vascular endothelial cells and macrophages in atherosclerotic lesions (36,37), but in the present study, LOX-1 was highly expressed not only in these cells, but also in FLS in the RA synovium (Figure 1). Importantly, the LOX-1 gene is an immediate early gene that processes the NF-κB response (11,13) and is dynamically modulated by proinflammatory mediators. Since LOX-1 is easily upregulated by cytokines, LOX-1 could have an important role in amplification of the local inflammatory response during systemic inflammation, as in RA. Therefore, blockade of the LOX-1 signal would be beneficial for the prevention of inflammation and cartilage destruction in RA.

The use of biologic agents yielded a paradigm shift in the treatment of RA. At present, the biologic treatments that are currently available target proinflammatory cytokines and lymphocytes; however, direct prevention of joint destruction is required, as the degree of physical disability in RA patients depends on the extent of joint destruction (38). In the present study, we showed, for the first time, that ox-LDL induces synovial inflammation and cartilage destruction in RA, and that this mechanism may be mediated by the production of MMP-3 and, possibly, MMP-1 in humans. Although MMP-3 (and MMP-1) may not be the only molecules produced from FLS via LOX-1 signaling, and they may not be uniquely responsible for the degradation of the cartilage, such a mechanism of ox-LDL–LOX-1 signaling, via the direct and potent induction of MMP-1 and MMP-3 from FLS, may render the anti–LOX-1 treatment unique in terms of its regulative abilities in both synovial inflammation and cartilage matrix degradation.

The lipid profiles and lipoprotein patterns observed in patients with RA are reportedly altered and may contribute to the high incidence of atherosclerotic CVD (39,40). This suggests that there is a common

pathophysiologic background between RA and atherosclerosis. Similar to what occurs in atherosclerosis, the lipids and lipoproteins present in the synovial fluid from inflamed joints in RA patients are oxidized (41), and the serum levels of ox-LDL are associated with the levels of disease activity in RA (42). We have previously shown that blockade of LOX-1 in animal models suppresses intimal hyperplasia after balloon injury and inhibits myocardial ischemia (43,44). Results from previous studies and those of the present study demonstrate that blockade of LOX-1 suppresses synovitis and cartilage destruction in the inflamed joints, as shown in zymosan-induced arthritis and ox-LDL–induced arthritis. In this study, sLOX-1 levels in the plasma and synovial fluid of RA patients were markedly elevated and were positively correlated with the extent of RA disease activity, similar to the findings reported previously in atherosclerotic diseases. Taken together, these results suggest that anti–LOX-1 therapy is highly potent in terms of preventing not only the destruction of the joints, but also the cardiovascular events that may occur in patients with RA.

One of the major limitations of this study was the lack of clinical trial data pertaining to LOX-1 blockade in human RA. Before such trials are initiated, mouse RA models should be used to validate the efficacy and side effects of a neutralizing anti–LOX-1 antibody and sLOX-1. Moreover, in this study, we administered a neutralizing anti–LOX-1 antibody and sLOX-1 directly into the knee joints. Further investigations are needed to estimate the effects of systemic administration on multiple joint swelling and joint cartilage destruction.

Although proinflammatory cytokines, such as TNFα, have profiles that are similar to those of ox-LDL in inflammation and cartilage degradation, we and others have reported that even proinflammatory cytokines have physiologic functions in homeostasis and tissue healing (45,46). Compared with the action of such cytokines, ox-LDL–LOX-1 signaling seems to play a major role in only a harmful way, thus lessening any concern regarding the undesirable side effects of anti–ox-LDL–LOX-1 treatments when compared with the side effects of anticytokine agents. Therefore, an anti–ox-LDL treatment that would achieve blockade of LOX-1 could be highly promising, as this signal is crucial for the fundamental inflammation that occurs during the pathophysiologic processes and degradation of joint cartilage in RA.

ACKNOWLEDGMENTS

We are grateful to Drs. T. Kakinuma, T. Hiramitsu, T. Kitaori, R. Tsutsumi, and K. Nishitani (Kyoto University Graduate School of Medicine) for their valuable technical assistance, and to Dr. M. Kobayashi (Kyoto University Graduate School of Medicine) for retrieving samples.

AUTHOR CONTRIBUTIONS

All authors were involved in drafting the article or revising it critically for important intellectual content, and all authors approved the final version to be published. Dr. Ito had full access to all of the data in the study and takes responsibility for the integrity of the data and the accuracy of the data analysis.

Study conception and design. Ito, Kume, Yasuda, Nakamura.

Acquisition of data. Ishikawa, Akiyoshi, Yoshitomi, Mitsuoka, Tanida, Murata, Shibuya, Kasahara, Kakino, Fujita.

Analysis and interpretation of data. Ishikawa, Ito, Kume, Yoshitomi, Sawamura.

REFERENCES

1. Smolen JS, Aletaha D, Koeller M, Weisman MH, Emery P. New therapies for treatment of rheumatoid arthritis. Lancet 2007;370:1861–74.
2. Scott DL, Wolfe F, Huizinga TW. Rheumatoid arthritis. Lancet 2010;376:1094–108.
3. Ribbens C, Martin y Porras M, Franchimont N, Kaiser MJ, Jaspar JM, Damas P, et al. Increased matrix metalloproteinase-3 serum levels in rheumatic diseases: relationship with synovitis and steroid treatment. Ann Rheum Dis 2002;61:161–6.
4. Del Rincon I, Williams K, Stern MP, Freeman GL, Escalante A. High incidence of cardiovascular events in a rheumatoid arthritis cohort not explained by traditional cardiac risk factors. Arthritis Rheum 2001;44:2737–45.
5. Boers M, Dijkmans B, Gabriel S, Maradit-Kremers H, O'Dell J, Pincus T. Making an impact on mortality in rheumatoid arthritis: targeting cardiovascular comorbidity. Arthritis Rheum 2004;50:1734–9.
6. Peters MJ, van Halm VP, Voskuyl AE, Smulders YM, Boers M, Lems WF, et al. Does rheumatoid arthritis equal diabetes mellitus as an independent risk factor for cardiovascular disease? A prospective study. Arthritis Rheum 2009;61:1571–9.
7. Ross R. Atherosclerosis is an inflammatory disease. Am Heart J 1999;138:419–20.
8. Memon RA, Staprans I, Noor M, Holleran WM, Uchida Y, Moser AH, et al. Infection and inflammation induce LDL oxidation in vivo. Arterioscler Thromb Vasc Biol 2000;20:1536–42.
9. Witztum JL, Steinberg D. Role of oxidized low density lipoprotein in atherogenesis. J Clin Invest 1991;88:1785–92.
10. Lourida ES, Georgiadis AN, Papavasiliou EC, Papathanasiou AI, Drosos AA, Tselepis AD. Patients with early rheumatoid arthritis exhibit elevated autoantibody titers against mildly oxidized low-density lipoprotein and exhibit decreased activity of the lipoprotein-associated phospholipase A2. Arthritis Res Ther 2007;9:R19.
11. Sawamura T, Kume N, Aoyama T, Moriwaki H, Hoshikawa H, Aiba Y, et al. An endothelial receptor for oxidized low-density lipoprotein. Nature 1997;386:73–7.
12. Kume N, Kita T. Lectin-like oxidized low-density lipoprotein receptor-1 (LOX-1) in atherogenesis. Trends Cardiovasc Med 2001;11:22–5.
13. Ogura S, Kakino A, Sato Y, Fujita Y, Iwamoto S, Otsui K, et al. LOX-1: the multifunctional receptor underlying cardiovascular dysfunction. Circ J 2009;73:1993–9.
14. Nakagawa T, Akagi M, Hoshikawa H, Chen M, Yasuda T, Mukai S, et al. Lectin-like oxidized low-density lipoprotein receptor 1 mediates leukocyte infiltration and articular cartilage destruction in rat zymosan-induced arthritis. Arthritis Rheum 2002;46:2486–94.
15. Kakinuma T, Yasuda T, Nakagawa T, Hiramitsu T, Akiyoshi M,

Akagi M, et al. Lectin-like oxidized low-density lipoprotein receptor 1 mediates matrix metalloproteinase 3 synthesis enhanced by oxidized low-density lipoprotein in rheumatoid arthritis cartilage. Arthritis Rheum 2004;50:3495–503.
16. Kume N, Murase T, Moriwaki H, Aoyama T, Sawamura T, Masaki T, et al. Inducible expression of lectin-like oxidized LDL receptor-1 in vascular endothelial cells. Circ Res 1988;83:322–7.
17. Sakurai K, Sawamura T. Stress and vascular responses. Endothelial dysfunction via lectin-like oxidized low-density lipoprotein receptor-1: close relationships with oxidative stress. J Pharmacol Sci 2003;91:182–6.
18. Murase T, Kume N, Kataoka H, Minami M, Sawamura T, Masaki T, et al. Identification of soluble forms of lectin-like oxidized LDL receptor-1. Arterioscler Thromb Vasc Biol 2000;20:715–20.
19. Kume N, Mitsuoka H, Hayashida K, Tanaka M, Kominami G, Kita T. Soluble lectin-like oxidized LDL receptor-1 (sLOX-1) as a sensitive and specific biomarker for acute coronary syndrome: comparison with other biomarkers. J Cardiol 2010;56:159–65.
20. Kume N, Mitsuoka H, Hayashida K, Tanaka M, Kita T. Soluble lectin-like oxidized low-density lipoprotein receptor-1 predicts prognosis after acute coronary syndrome: a pilot study. Circ J 2010;74:1399–404.
21. Hayashida K, Kume N, Murase T, Minami M, Nakagawa D, Inada T, et al. Serum soluble lectin-like oxidized low-density lipoprotein receptor-1 levels are elevated in acute coronary syndrome: a novel marker for early diagnosis. Circulation 2005;112:812–8.
22. Mehta JL, Sanada N, Hu CP, Chen J, Dandapat A, Sugawara F, et al. Deletion of LOX-1 reduces atherogenesis in LDLR knockout mice fed high cholesterol diet. Circ Res 2007;100:1634–42.
23. Inoue N, Okamura T, Kokubo Y, Fujita Y, Sato Y, Nakanishi M, et al. LOX index, a novel predictive biochemical marker for coronary heart disease and stroke. Clin Chem 2010;56:550–8.
24. Arnett FC, Edworthy SM, Bloch DA, McShane DJ, Fries JF, Cooper NS, et al. The American Rheumatism Association 1987 revised criteria for the classification of rheumatoid arthritis. Arthritis Rheum 1988;31:315–24.
25. Prevoo ML, van 't Hof MA, Kuper HH, van Leeuwen MA, van de Putte LB, van Riel PL. Modified disease activity scores that include twenty-eight–joint counts: development and validation in a prospective longitudinal study of patients with rheumatoid arthritis. Arthritis Rheum 1995;38:44–8.
26. Nakamura M, Ohta H, Kume N, Hayashida K, Tanaka M, Mitsuoka H, et al. Generation of monoclonal antibodies against a soluble form of lectin-like oxidized low-density lipoprotein receptor-1 and development of a sensitive chemiluminescent enzyme immunoassay. J Pharm Biomed Anal 2010;51:158–63.
27. Bar-Yehuda S, Rath-Wolfson L, Del Valle L, Ochaion A, Cohen S, Patoka R, et al. Induction of an antiinflammatory effect and prevention of cartilage damage in rat knee osteoarthritis by CF101 treatment. Arthritis Rheum 2009;60:3061–71.
28. Coles JM, Zhang L, Blum JJ, Warman ML, Jay GD, Guilak F, et al. Loss of cartilage structure, stiffness, and frictional properties in mice lacking PRG4. Arthritis Rheum 2010;62:1666–74.
29. Cunnane G, FitzGerald O, Hummel KM, Youssef PP, Gay RE, Gay S, et al. Synovial tissue protease gene expression and joint erosions in early rheumatoid arthritis. Arthritis Rheum 2001;44:1744–53.
30. Molenaar ET, Voskuyl AE, Dinant HJ, Bezemer PD, Boers M, Dijkmans BA. Progression of radiologic damage in patients with rheumatoid arthritis in clinical remission. Arthritis Rheum 2004;50:36–42.
31. Aletaha D, Neogi T, Silman AJ, Funovits J, Felson DT, Bingham CO III, et al. 2010 rheumatoid arthritis classification criteria: an American College of Rheumatology/European League Against Rheumatism collaborative initiative. Arthritis Rheum 2010;62:2569–81.
32. Lubrano V, Del Turco S, Nicolini G, Di Cecco P, Basta G. Circulating levels of lectin-like oxidized low-density lipoprotein receptor-1 are associated with inflammatory markers. Lipids 2008;43:945–50.
33. Bizzaro N, Mazzanti G, Tonutti E, Villalta D, Tozzoli R. Diagnostic accuracy of the anti-citrulline antibody assay for rheumatoid arthritis. Clin Chem 2001;47:1089–93.
34. Keenan RT, Swearingen CJ, Yazici Y. Erythrocyte sedimentation rate and C-reactive protein levels are poorly correlated with clinical measures of disease activity in rheumatoid arthritis, systemic lupus erythematosus and osteoarthritis patients. Clin Exp Rheumatol 2008;26:814–9.
35. Nakagawa T, Yasuda T, Hoshikawa H, Shimizu M, Kakinuma T, Chen M, et al. LOX-1 expressed in cultured rat chondrocytes mediates oxidized LDL-induced cell death: possible role of dephosphorylation of Akt. Biochem Biophys Res Commun 2002;299:91–7.
36. Tiwari RL, Singh V, Barthwal MK. Macrophages: an elusive yet emerging therapeutic target of atherosclerosis. Med Res Rev 2008;28:483–544.
37. Chen M, Masaki T, Sawamura T. LOX-1, the receptor for oxidized low-density lipoprotein identified from endothelial cells: implications in endothelial dysfunction and atherosclerosis. Pharmacol Ther 2002;95:89–100.
38. Breedveld FC, Han C, Bala M, van der Heijde D, Baker D, Kavanaugh AF, et al. Association between baseline radiographic damage and improvement in physical function after treatment of patients with rheumatoid arthritis. Ann Rheum Dis 2005;64:52–5.
39. Choi HK, Seeger JD. Lipid profiles among US elderly with untreated rheumatoid arthritis: the Third National Health and Nutrition Examination Survey. J Rheumatol 2005;32:2311–6.
40. Dursunoglu D, Evrengul H, Polat B, Tanriverdi H, Cobankara V, Kaftan A, et al. Lp(a) lipoprotein and lipids in patients with rheumatoid arthritis: serum levels and relationship to inflammation. Rheumatol Int 2005;25:241–5.
41. Winyard PG, Tatzber F, Esterbauer H, Kus ML, Blake DR, Morris CJ. Presence of foam cells containing oxidised low density lipoprotein in the synovial membrane from patients with rheumatoid arthritis. Ann Rheum Dis 1993;52:677–80.
42. Kim SH, Lee CK, Lee EY, Park SY, Cho YS, Yoo B, et al. Serum oxidized low-density lipoproteins in rheumatoid arthritis. Rheumatol Int 2004;24:230–3.
43. Hinagata J, Kakutani M, Fujii T, Naruko T, Inoue N, Fujita Y, et al. Oxidized LDL receptor LOX-1 is involved in neointimal hyperplasia after balloon arterial injury in a rat model. Cardiovasc Res 2006;69:263–71.
44. Li D, Williams V, Liu L, Chen H, Sawamura T, Antakli T, et al. LOX-1 inhibition in myocardial ischemia-reperfusion injury: modulation of MMP-1 and inflammation. Am J Physiol Heart Circ Physiol 2002;283:1795–801.
45. Lange J, Sapozhnikova A, Lu C, Hu D, Li X, Miclau T 3rd, et al. Action of IL-1β during fracture healing. J Orthop Res 2010;28:778–84.
46. Nishitani K, Ito H, Hiramitsu T, Tsutsumi R, Tanida S, Kitaori T, et al. PGE2 inhibits MMP expression by suppressing MKK4-JNK MAP kinase-c-JUN pathway via EP4 in human articular chondrocytes. J Cell Biochem 2010;109:425–33.

OPEN ACCESS Freely available online

PLoS one

Stromal Cell-Derived Factor 1 Regulates the Actin Organization of Chondrocytes and Chondrocyte Hypertrophy

Koichi Murata[1]*, Toshiyuki Kitaori[1]*, Shinya Oishi[2], Naoki Watanabe[3], Hiroyuki Yoshitomi[1], Shimei Tanida[1], Masahiro Ishikawa[1], Takashi Kasahara[1], Hideyuki Shibuya[1], Nobutaka Fujii[2], Takashi Nagasawa[4], Takashi Nakamura[1], Hiromu Ito[1,5]

1 Department of Orthopaedic Surgery, Kyoto University Graduate School of Medicine, Sakyo, Kyoto, Japan, **2** Department of Chemogenomics, Kyoto University Graduate School of Pharmaceutical Sciences, Kyoto, Japan, **3** Laboratory of Single-Molecule Cell Biology, Tohoku University Graduate School of Life Science, Aoba, Sendai, Japan, **4** Department of Immunobiology and Hematology, Kyoto University, Institute for Frontier Medical Sciences, Kyoto, Japan, **5** Department of the Control for Rheumatic Diseases, Kyoto University Graduate School of Medicine, Kyoto, Japan

Abstract

Stromal cell-derived factor 1 (SDF-1/CXCL12/PBSF) plays important roles in the biological and physiological functions of haematopoietic and mesenchymal stem cells. This chemokine regulates the formation of multiple organ systems during embryogenesis. However, its roles in skeletal development remain unclear. Here we investigated the roles of SDF-1 in chondrocyte differentiation. We demonstrated that SDF-1 protein was expressed at pre-hypertrophic and hypertrophic chondrocytes in the newly formed endochondral callus of rib fracture as well as in the growth plate of normal mouse tibia by immunohistochemical analysis. Using SDF-$1^{-/-}$ mouse embryo, we histologically showed that the total length of the whole humeri of SDF-$1^{-/-}$ mice was significantly shorter than that of wild-type mice, which was contributed mainly by shorter hypertrophic and calcified zones in SDF-$1^{-/-}$ mice. Actin cytoskeleton of hypertrophic chondrocytes in SDF-$1^{-/-}$ mouse humeri showed less F-actin and rounder shape than that of wild-type mice. Primary chondrocytes from SDF-$1^{-/-}$ mice showed the enhanced formation of philopodia and loss of F-actin. The administration of SDF-1 to primary chondrocytes of wild-type mice and SDF-$1^{-/-}$ mice promoted the formation of actin stress fibers. Organ culture of embryonic metatarsals from SDF-$1^{-/-}$ mice showed the growth delay, which was recovered by an exogenous administration of SDF-1. mRNA expression of type X collagen in metatarsals and in primary chondrocytes of SDF-$1^{-/-}$ mouse embryo was down-regulated while the administration of SDF-1 to metatarsals recovered. These data suggests that SDF-1 regulates the actin organization and stimulates bone growth by mediating chondrocyte hypertrophy.

Citation: Murata K, Kitaori T, Oishi S, Watanabe N, Yoshitomi H, et al. (2012) Stromal Cell-Derived Factor 1 Regulates the Actin Organization of Chondrocytes and Chondrocyte Hypertrophy. PLoS ONE 7(5): e37163. doi:10.1371/journal.pone.0037163

Editor: Jialin Charles Zheng, University of Nebraska Medical Center, United States of America

Received November 8, 2011; **Accepted** April 16, 2012; **Published** May 18, 2012

Funding: This work was supported by Grant-in-Aids from the Ministry of Education of Japan (No. 19591756 and No.21591942). The funders had no role in study design, data collection and analysis, decision to publish, or preparation of the manuscript.

Competing Interests: The authors have declared that no competing interests exist.

* E-mail: hiromu@kuhp.kyoto-u.ac.jp

Introduction

Endochondral ossification is an essential process for skeletal development [1]. During skeletogenesis, mesenchymal cells aggregate at the sites where skeletal elements will eventually be formed, and they differentiate into chondrocytic lineage and proliferate. The cartilage templates are composed of nonhypertrophic (resting and proliferating) and hypertrophic chondrocytes as well as vast amounts of extracellular matrix produced by chondrocytes [1]. Chondrocyte hypertrophy is a unique step in chondrocyte differentiation, in which the cells become bigger and rather transparent, and is a mandatory event allowing calcification, vascularization, osteoblast differentiation, and remodeling into bone to occur [2].

A number of secreted or intracellular polypeptides cooperatively regulate the transition of chondrocyte hypertrophy. PTH-related peptide, Indian hedgehog, fibroblast growth factors, SRY (sex determining region Y)-box 9 (Sox9) and Wnt proteins are reportedly essential factors for chondrocyte hypertrophy [3–8]. However, much less is known about the intracellular events, such as cytoskeletal reorganization that can allow the cell size and shape to change.

Stromal cell-derived factor-1 (SDF-1)/pre-B cell growth-stimulating factor belongs to CXC subfamily of chemokines as CXCL12 [9,10]. SDF-1 signals through a G-protein-coupled receptor, C-X-C chemokine receptor 4 (CXCR4) [10,11] and, CXCR7 [12,13], and critical roles of SDF-1/CXCR4 in hematopoietic stem cells (HSCs) have been extensively reported.

During the last decade, accumulating data have supported an emerging hypothesis that SDF-1/CXCR4 also plays pivotal roles in the biological and physiological functions of mesenchymal stem cells (MSCs) [14,15]. SDF-1 is up-regulated at sites of injuries and serves as a potent chemoattractant to recruit circulating or residing CXCR4-expressing MSCs which are necessary for a tissue-specific organ repair or regeneration in liver [16], heart [17,18], brain [19], kidney [20], and skin [21]. We have recently demonstrated

that SDF-1 recruited MSCs to bone repairing sites in the acute phase of endochondral bone repair [22]. However, little is known on roles of SDF-1/CXCR4 signal on the bone growth and the endochondral bone formation.

In the process of chondrogenesis, chondrocytes change cell shape from a fibroblastoid to a round or polygonal morphology, which is called as hypertrophic conversion [23], a unique and crucial step in chondrocyte differentiation. The molecular mechanisms responsible for this cell shape change are largely unknown, but the actin cytoskeleton presumably plays important roles in this context. The only intracellular signaling known to associate with the actin reorganization during chondrocyte differentiation is RhoA/ROCK [24–26]. The reports on RhoA/ROCK suggest that the changes in morphology have important roles in chondrocyte differentiation. On the other hand, SDF-1 induces cytoskeleton rearrangements in homing and migration of hematopoietic cells through Phosphoinositide 3-kinase/Akt and RhoA/ROCK signaling [27,28], which can lead to an assumption of the important roles of SDF-1 on the shape and size changes of chondrocytes. This assumption, however, remains to be largely investigated.

We herein demonstrated that SDF-1 is crucial for endochondral bone development. The embryonic humeri of SDF-$1^{-/-}$ mice were shorter than those of wild-type mice, especially prominent in the hypertrophic zone. The actin cytoskeleton of SDF-$1^{-/-}$ chondrocytes in the humeri and in monolayer culture was disturbed. With cultured metatarsal explants of SDF-$1^{-/-}$mice, the lack of SDF-1 impaired the development of metatarsals and chondrocyte hypertrophy, and the addition of SDF-1 reversed the impairments. Our results strongly suggest that SDF-1 regulates actin polymerization and stimulates bone growth by mediating chondrocyte hypertrophy.

Results

Distribution of SDF-1 in the Growth Plate and the Endochondral Callus

To evaluate potential roles of SDF-1 in endochondral bone formation, we analyzed the distribution of SDF-1 in the tibial growth plates from 4-week-old wild-type mice and newly formed endochondral callus of rib fracture model at day 10 by immunohistochemistry. SDF-1 was expressed at prehypertrophic and hypertrophic chondrocytes both in the growth plate (**Figure 1A**) and in the endochondral callus (**Figure 1B**), suggesting important roles of SDF-1 on the transition from prehypertrophic to hypertrophic chondrocytes in endochondral bone formation.

Delayed Growth and Reduced Size of the Hypertrophic Zone of SDF-$1^{-/-}$ Mouse Humeri

To investigate the effect of SDF-1 in endochondral bone formation, we next evaluated the phenotypic differences between SDF-$1^{-/-}$ and wild-type mice. The humeri were resected from embryos at E13.5, E14.5, E15.5, and E16.5 (n = 4 at each point), and processed in paraffin sections (**Figure 2A**). The lengths of the total humeri and the ratios of proliferating, hypertrophic, and calcified zones were measured (**Figure 2B**). The total length of the whole humerus of SDF-$1^{-/-}$ mice was shorter than that of wild-type mice in E14.5, E15.5, and E16.5 by 17.9%, 24.7%, and 6.8%, respectively, with statistical significances. To examine which zone contributed to the total length difference, we evaluated the proliferating, hypertrophic, and calcified zones of the humeri as the percentages against the total length. The ratio of hypertrophic zone was significantly smaller in SDF-$1^{-/-}$ mice than in wild-type mice at E14.5 and E15.5 by 21.2% and 31.0%, respectively. The ratio of calcified zone was also smaller in SDF-$1^{-/-}$ mice than in wild-type mice at E14.5 and E15.5 by 45.0% and 36.0%, respectively, with statistical significances. The most marked difference was found at E15.5, especially in the hypertrophic zone, while no significant differences were observed in any zones at E13.5. No significant difference was found in cell proliferation rates between SDF-$1^{-/-}$ and wild-type mice based on 5-Bromo-2′ deoxy-uridine (Brd-U) staining (**Figure S1**). These results demonstrated the absence of SDF-1 mainly affects the growth of the hypertrophic zone rather than the proliferating zone.

Absence of SDF-1 Impairs Cytoskeleton of Hypertrophic Chondrocytes

SDF-1 signaling leads to cytoskeleton rearrangements and integrin activation in hematopoietic cells [27]. Chondrocytes change their shape drastically from a fibroblastoid to a round shape during chondrogenesis. The reorganization of the actin cytoskeleton is also demonstrated to be important in hypertrophic transition of chondrocytes [24]. To determine whether SDF-1 affects the reorganization of the actin cytoskeleton and cellular morphology, we stained the frozen sections of the humeri from SDF-$1^{-/-}$ and wild-type mouse embryos (E15.5) with Rhodamine-Phalloidin. No clear difference between SDF-$1^{-/-}$ and wild-type hypertrophic chondrocytes was detected in the HE staining (data not shown) and in the differentiation interference image (**Figure 3A**). But interestingly, the Rhodamine-Phalloidin staining showed that the hypertrophic chondrocytes in SDF-$1^{-/-}$ mice was rounder than wild-type mice. Quantification of F-actin revealed that F-actin content of hypertrophic chondrocytes in SDF-$1^{-/-}$ mice was significantly lower than wild-type mice ($P<0.05$, **Figure 3B**). Next, to measure the ellipticity of chondrocytes, we calculated the ratio of a short axis to the long axis (1/ellipticity). The reciprocal of ellipticity was significantly higher in SDF-$1^{-/-}$ chondrocytes than in wild-type chondrocytes ($P<0.05$, **Figure 3C**), which support the roundness of SDF-$1^{-/-}$ hypertrophic chondrocytes. These tendencies were also observed in hypertrophic chondrocytes of SDF-$1^{-/-}$ metatarsals (data not shown).

SDF-1 Controls the Actin Organization of Primary Chondrocytes

Based on the results described above, we investigated whether SDF-1 regulates the actin cytoskeleton of the chondrocytes, F-actin of primary chondrocytes were stained with Rhodamine-Phalloidin. Untreated chondrocytes from wild-type mice had a defined cortical rim, minimal stress fibers, and a polyhedral shape (**Figure 4**). With treatment of SDF-1 (100 ng/ml), the chondrocytes changed their shape into contractile rounded shape in a time-dependent manner. Incubation of the chondrocytes for 10 m with SDF-1 showed the actin stress fiber formation.

Next, wild-type primary chondrocytes were treated with SDF-1, or SDF-1 and CXCR4 specific antagonist, TF14016 [29] (100 μM), or pertussis toxin (PTX, 100 ng/ml) for 60 m (**Figure 5A**). Treatment with SDF-1 to primary chondrocytes resulted in contractile rounded cells with thick cortical rim of actin filaments. The chondrocytes treated with SDF-1 and TF14016 showed the similar morphology to untreated chondrocytes. Cells treated with SDF-1 and PTX showed slight induction of actin stress fibers. In quantitation of the F-actin in the Rhodamine-Phalloidin-stained cells, the F-actin content treated with SDF-1 for 60 m was significantly higher than the actin density of the

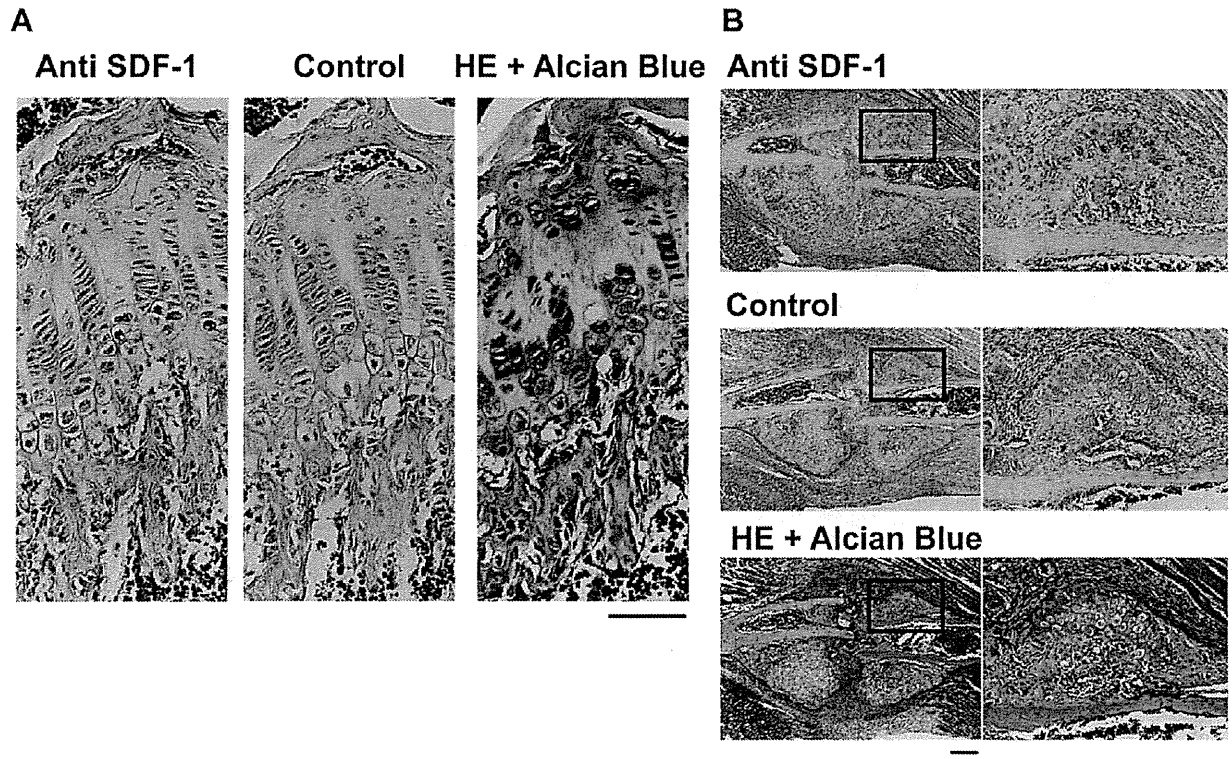

Figure 1. SDF-1 protein was expressed at the prehypertrophic and hypertrophic zones. The growth plate of 4-week-old mouse tibia (A) and endochondral callus of rib fracture (B) were stained with hematoxylin and eosin (HE), or immunohistochemically stained with antiSDF-1 antibody or IgG (control). Boxed areas in the panel are shown in a higher magnification (×200) in the right panels. The result is representative of three separate experiments; Scale bar, 200 μm.
doi:10.1371/journal.pone.0037163.g001

chondrocytes treated with either medium alone, SDF-1+PTX, or SDF-1+TF14016 (**Figure 5B**).

Then we investigated the actin filaments of primary chondrocytes from SDF-$1^{-/-}$ mice. Those chondrocytes clearly showed the enhanced formation of philopodia and the lost of F-actin through 7-day culture, compared with those of wild-type mice. The administration of recombinant SDF-1 to the chondrocytes of SDF-$1^{-/-}$ mice inhibited the philopodia formation and the loss of F-actin. The cortical rim and shape of SDF-$1^{-/-}$ chondrocytes with recombinant SDF-1 was similar to that of wild-type chondrocytes (**Figure 5C**). Quantification of F-actin revealed that actin density of SDF-$1^{-/-}$ chondrocytes was lower than that of wild-type chondrocytes and of SDF-$1^{-/-}$ chondrocytes incubated with recombinant SDF-1 ($P<0.01$, $P<0.05$, respectively) (**Figure 5D**). These results suggest that SDF-1/CXCR4 signaling strongly affects the reorganization of the actin cytoskeleton and the cellular morphology in primary chondrocytes.

Deficit of SDF-1/CXCR4 Signaling Delays the Growth of Metatarsals in Organ Culture

The phenotypic changes of SDF-$1^{-/-}$ mice exclusively occurred from E14.5 to E16.5. This period corresponds to the time of the vascular invasion, which indicates that molecular and/or cellular factors from circulation compensate for the lack of SDF-1. To verify the independent effects of endogenous SDF-1 in pre-vascularized bone, we used the primary metatarsal explant culture system. The metatarsal bones were harvested from wild-type mice at E15.5, cultured for 7 days, and the total length was measured at day 1, 3, 5 and 7 (**Figure 6**). We first confirmed that no vascular formation was observed in metatarsal bones at this stage by histology (data not shown).

As shown in **Figure 6A**, the metatarsal bones of wild-type mice kept up growing during the whole culture period and the ratio of the total length growth reached to 134% at day 7. The growth delayed at every time point in SDF-1+/− and SDF-$1^{-/-}$ mice, and the ratios of the total length growth remained 128% and 121% at day 7, respectively. At the end of this culture assay, the total length of SDF-$1^{-/-}$ metatarsal bones was 9.7% shorter than wild-type metatarsals with statistical significance, indicating the functional effect of endogenous SDF-1 in the normal bone growth. Then, to investigate whether SDF-1 can restore the perturbed growth of SDF-$1^{-/-}$ metatarsal bones, 100 ng/ml of SDF-1 was added to the primary metatarsal culture system. The treatment of SDF-1 significantly regained the ratio of the total length growth of SDF-$1^{-/-}$ metatarsals from 124% to 137% at day 7, which was the similar growth rate of wild-type metatarsals. Interestingly, during this assay, we observed calcified zones, verified by von Kossa staining, were found in 80.0%, 69.2%, and 16.7% of wild-type, SDF-1+/−, and SDF-$1^{-/-}$ metatarsals, respectively at day 7 (**Figures 6B, C**), indicating that the delayed differentiation of hypertrophic chondrocytes affects the calcification of those cells in SDF-$1^{-/-}$ mice, which was consistent with the phenotype of the SDF-$1^{-/-}$ humerus (**Figure 2**).

These results strongly support the notion that self-produced SDF-1 is crucial for endochondral bone development at the pre-vascularized stage.

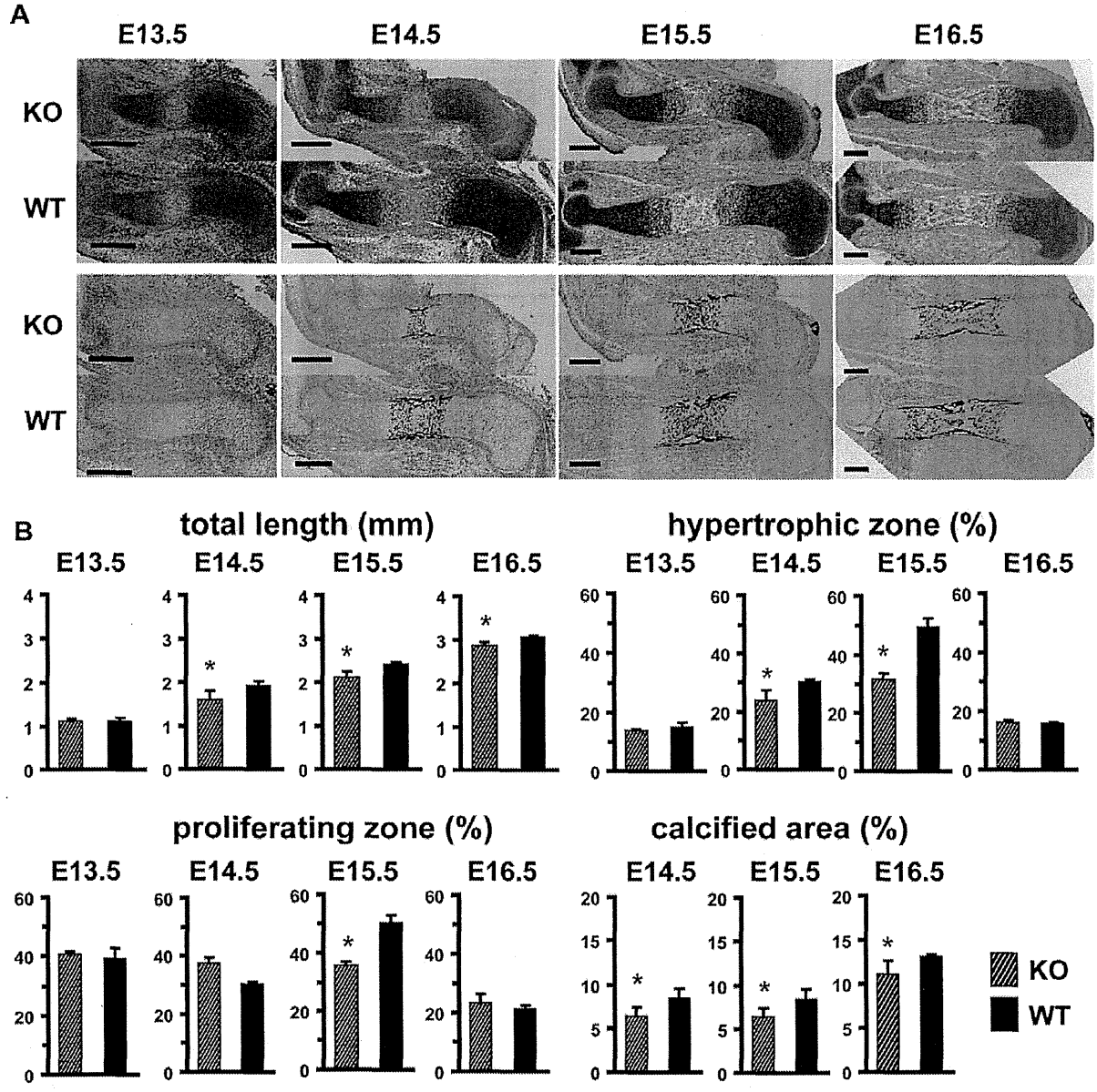

Figure 2. Growth of the embryonic humeri of SDF-1$^{-/-}$ mice delays. A: The embryonic humeri of wild-type (WT) and SDF-1$^{-/-}$ (KO) mice. Specimens were processed to paraffin-embedded sections and stained with hematoxylin, eosin (lower panels) and alcian blue (upper panels). **B**: Length of the humeri. The total length of the humeri and the ratios of the proliferating, the hypertrophic, or the calcified zone in each day were calculated as described in Methods section. Values are the mean and standard deviation of more than three independent experiments; *, $P<0.05$; Scale bar, 300 μm.
doi:10.1371/journal.pone.0037163.g002

SDF-1 Deficiency Impairs Type X Collagen Gene Expression

To examine the effect of SDF-1 to the phenotypical expression of type X collagen (Col X), and Sox9, metatarsal bones from E15.5 wild-type and SDF-1$^{-/-}$ mouse embryos were cultured with or without SDF-1 for 3 or 7 days, and total RNAs were extracted and quantified by real-time PCR.

The expression of Col X mRNA increased from day 3 to day 7 in untreated wild-type metatarsals (**Figure 6D**), which demonstrated the normal growth of the explant culture. The expression of Col X mRNA decreased significantly at day 7 in untreated SDF-1$^{-/-}$ metatarsals. The administration of recombinant SDF-1 to SDF-1$^{-/-}$ metatarsals recovered the expression of Col X. There was no statistically significant difference in Sox9 expression.

Furthermore, primary chondrocytes isolated from wild-type and SDF-1$^{-/-}$ mice were cultured for 3 weeks in chondrogenic medium supplemented with insulin to induce chondrocyte differentiation. Chondrocytes from SDF-1$^{-/-}$ mice showed decreased Col X expression compared with that from wild-type mice (**Figure 6E**). The expression of Sox9 showed no statistically significant difference.

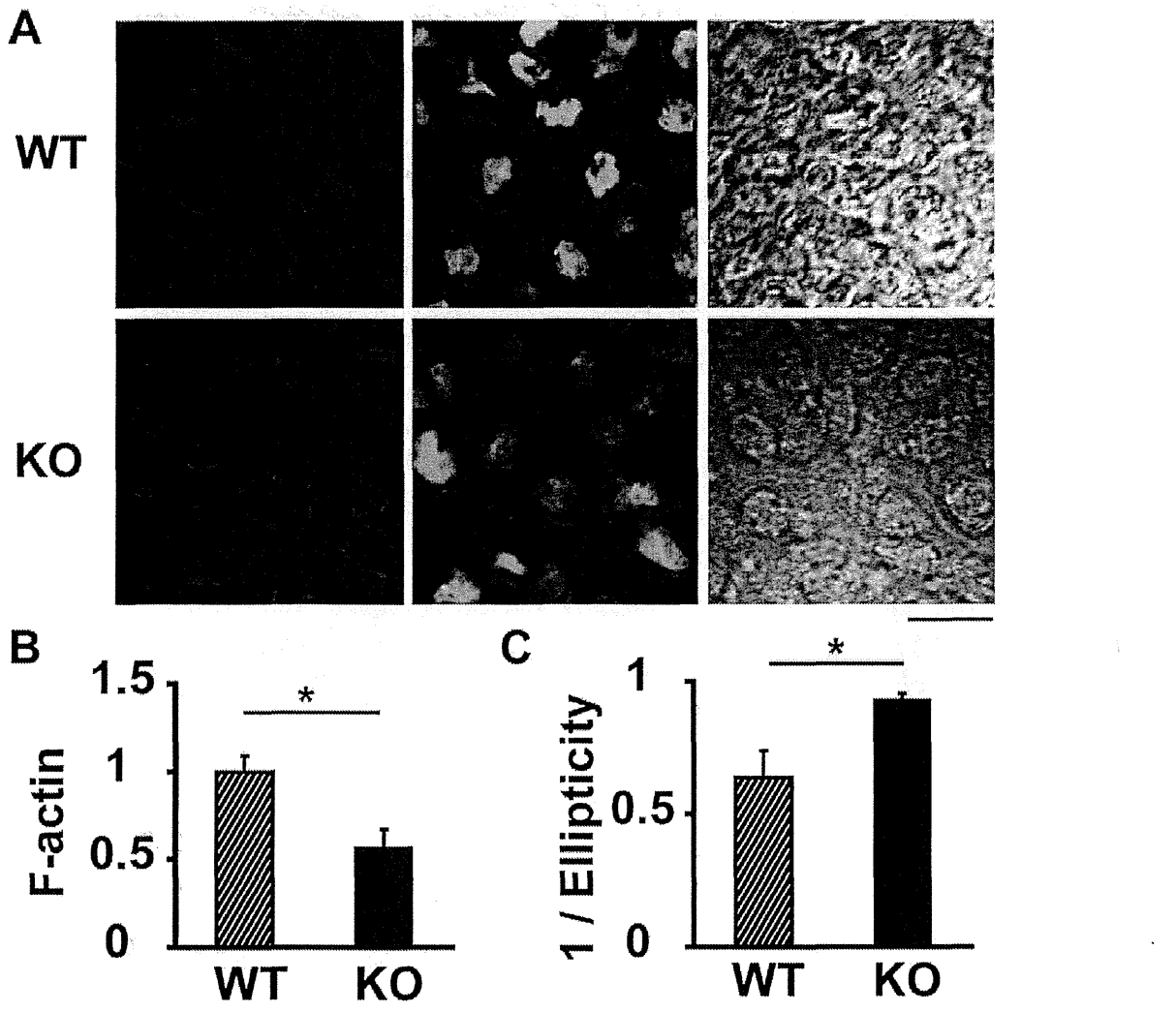

Figure 3. Cytoskeleton of hypertrophic chondrocytes in the humeri. A: Frozen sections of the humeri isolated from SDF-1$^{-/-}$ (KO), and wild-type (WT) mice at E15.5, were fixed with paraformaldehyde and stained with Rhodamine-Phalloidin for actin filaments and SYBR Green for nuclei. Left panel, Rhodamine-Phalloidin; middle panel, merge of Rhodamine-Phalloidin and SYBR Green; right panel, differentiation interference image. Representative fields are shown. **B**: The intensity of actin filament staining (F-actin) was quantified with Image J software. Values were normalized to F-actin of WT chondrocytes. **C**: The ratios of the short axis to the long axis (1/Ellipticity) in chondrocytes were calculated with Image J. Values are the mean and s.e.m. of more than three separate experiments; *, $P<0.05$; Scale bar, 10 μm.
doi:10.1371/journal.pone.0037163.g003

Discussion

SDF-1/CXCR4 plays important roles in the biological and physiological functions of MSCs [14,15], serving as a potent chemoattractant to recruit circulating or residing CXCR4-expressing MSCs to injured organs [16–21], including the fracture site of bones [22]. SDF-1 also plays crucial roles in the formation of multiple organ systems during embryogenesis [30–32], and it has been shown to associate with several diseases involving the skeleton, including rheumatoid arthritis and cancers that metastasize to the bone [33,34]. In the present study we showed, for the first time, the promotion of chondrocyte hypertrophy with SDF-1 and contribution of SDF-1 to the actin reorganization, which had been shown to be important for chondrocyte differentiation.

During the endochondral bone development, SDF-1 is expressed at the growth plate, but the precise localization of SDF-1 in the growth plate is controversial. A previous study showed that SDF-1 was expressed in the central region of the proliferating zone of the growth plate at E14.5 and it was expressed in the periosteum and central region of the proliferating zone at E16.5 [35]. On the other hand, another study showed that SDF-1 was expressed in the area adjacent to the hypertrophic zone of the growth plate [36]. Immunohistochemical analysis of the current study revealed that SDF-1 protein was expressed in hypertrophic chondrocytes of the growth plates of the tibia and the fracture callus (**Figure 1**) as well as the hypertrophic zone of mouse embryos (data not shown). These data suggest that SDF-1 has important, physiological roles in the hypertrophic zone during the endochondral bone formation even after birth.

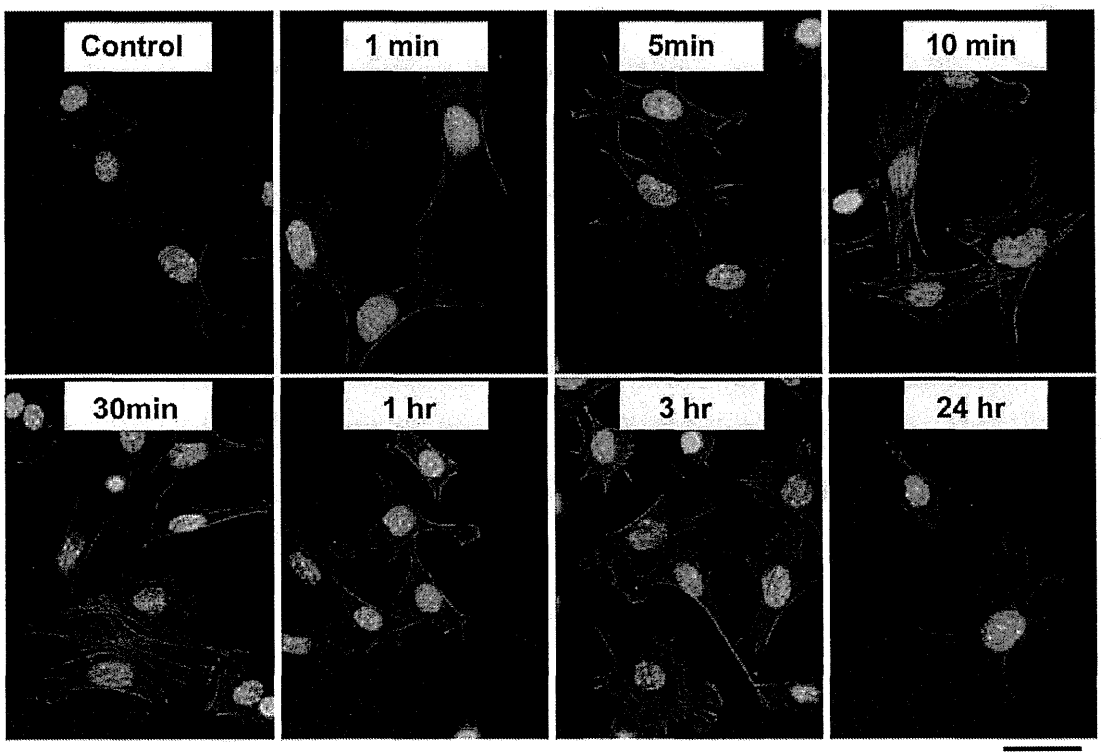

Figure 4. SDF-1 simulates actin assembly and stress fiber formation in a time-dependent manner. Primary chondrocytes from wild-type mice were treated with SDF-1 (100 ng/ml) as indicated. Cells were then fixed with paraformaldehyde and stained with Rhodamine-Phalloidin for actin filaments and 4′,6-diamidino-2-phenylindole for nuclei; Scale bar, 20 μm.
doi:10.1371/journal.pone.0037163.g004

SDF-1 is involved in the migration of hematopoietic progenitors and morphogenesis of leukocytes [37]. In the processes, SDF-1 induces morphological changes in adherent leukocytes and the acquisition of a bipolar shape with front leading edges [38,39], by stimulating the actin polymerization in a Rac and Cdc42-dependent fashion [38], and activating the small GTPases that control the actin cytoskeleton [40]. On the other hand, the actin cytoskeleton plays important roles in cellular homeostasis, proliferation and differentiation [41,42]. Even in the hypertrophic transition during chondrocyte differentiation, chondrocytes change the cell shape from a fibroblastoid to a round or polygonal morphology [23] and, as an upstream regulator of cytoskeletal dynamics, RhoA/ROCK signaling was shown to associate with chondrocyte hypertrophy [43]. In this study, incubation of wild-type and SDF-$1^{-/-}$ chondrocytes with SDF-1 changed the cell shape with an increase of F-actin density (**Figure 4**). In accordance with this fact, actin cytoskeletons of wild-type and SDF-$1^{-/-}$ hypertrophic chondrocytes in the humeri were different in the amount and the shape (**Figure 3**). These results suggest that SDF-1 signaling affects the reorganization of the actin cytoskeleton and the maintenance of the cellular morphology.

Phenotypic changes of SDF-$1^{-/-}$ hypertrophic chondrocytes of the humeri were mostly observed from E14.5 to E15.5, and the significant difference was lost at E16.5 (**Figure 2**). As we observed the vascularization of the humeri at E15.5 with the expression of SDF-1, we assume that the shortness of the humeri of SDF-$1^{-/-}$ mice is compensated by the effects of circulating factors from blood after neovascularization occurs. To exclude the effect of the vascularization of the humeri, the organ culture of metatarsal bones was performed, and we found that the bone growth was disturbed by lack of SDF-1, and that the discretion was rescued by the administration of SDF-1. These results suggest that SDF-1 is crucial in chondrocyte differentiation at the prevascularized stage, and the functions of SDF-1 in chondrocyte differentiation are totally apart from roles on the recruitment of MSCs nor HSCs.

The bone growth is driven primarily by the rate of production of hypertrophic chondrocytes from proliferating chondrocytes [44]. In the metatarsal explant culture, lack of SDF-1 resulted in the decreased expression of Col X with disturbance of the bone growth (**Figures 6A, D**). This fact suggests SDF-1 signaling is important for the hypertrophic conversion of proliferating chondrocytes. Interestingly, the appearance of the calcified zones was delayed in the explant culture of SDF-$1^{-/-}$ mice (**Figures 5B, C**). Since the hypertrophic conversion is a prerequisite of calcification of chondrocytes, SDF-1 is suggestively crucial on the hypertrophic conversion and the subsequent calcification of chondrocytes. Indeed, the delayed calcification was also found in the SDF-$1^{-/-}$ humeri (**Figure 2A**), and the disturbed hypertrophic conversion led to the shortness of calcified zones as well as that of the hypertrophic zones in SDF-$1^{-/-}$ mouse embryos (**Figure 2B**). Furthermore, the stimulation of SDF-1 to SDF-$1^{-/-}$ metatarsals increased the expression of Col X mRNA (**Figure 6D**). Since SDF-1 is expressed at prehypertrophic and hypertrophic chondrocytes (**Figure 1**) with CXCR4 expression being the strongest in the hypertophic chondrocytes [**36**], the effects of SDF-1 on chondrocyte differentiation may have occurred mainly in the prehypertrophic and hypertrophic zones as enhancement of chondrocyte hypertrophy.

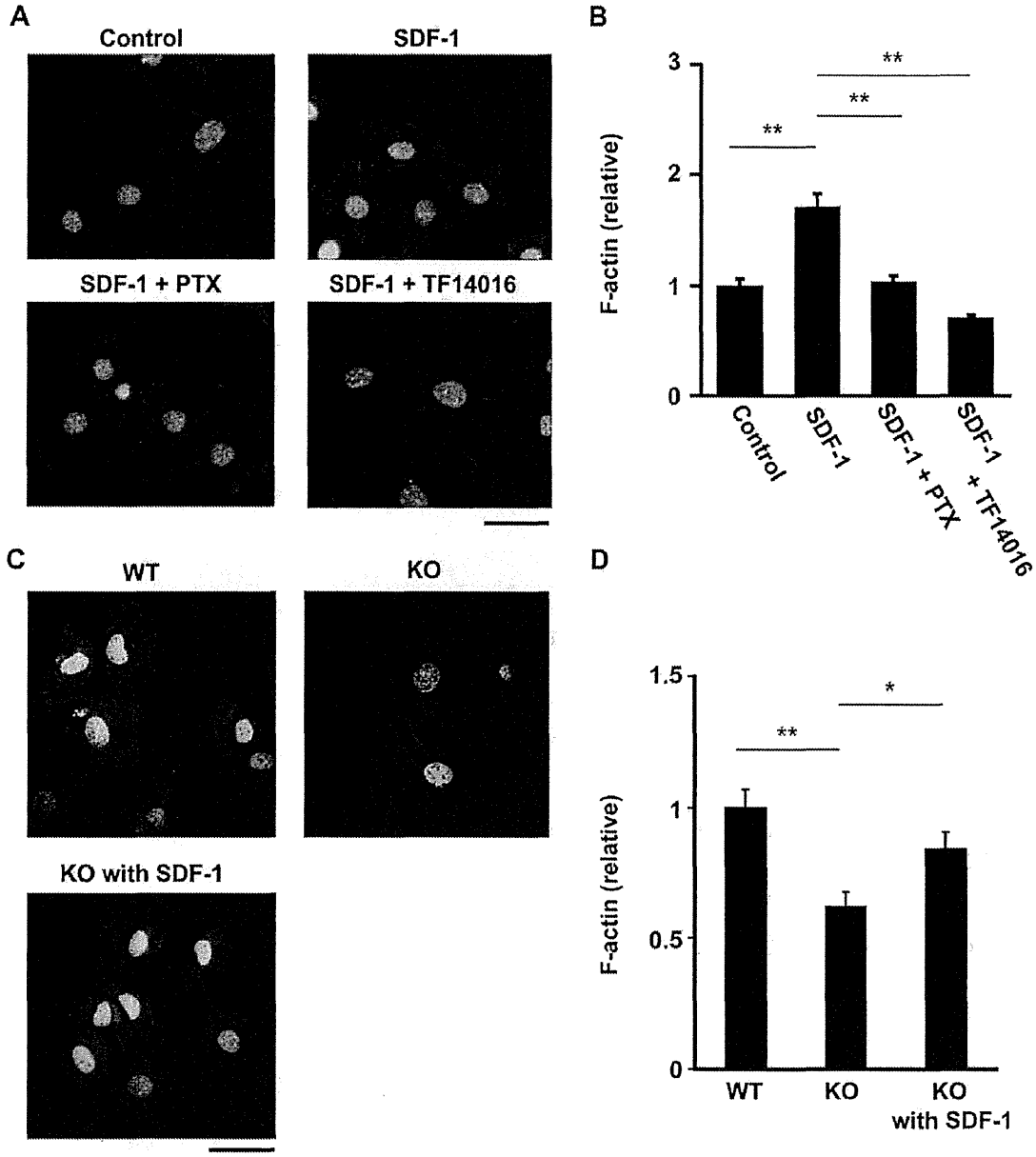

Figure 5. SDF-1/CXCR4 pathway controls actin cytoskeleton. A: Treatment with SDF-1 increased the actin filament density in primary chondrocytes. Primary chondrocytes from wild-type mice were treated with SDF-1 (100 ng/ml), or SDF-1 and CXCR4 specific antagonist, TF14016 (100 μM) or pertussis toxin (PTX, 100 ng/ml) for 60 m and stained with Rhodamine-Phalloidin. **B**: The F-actin content in chondrocytes was analyzed with Image J software. All values were normalized to F-actin of chondrocytes treated with conditioned medium only. **C**: Actin cytoskeleton of primary chondrocyte from SDF-1$^{-/-}$ (KO), and wild-type (WT) mice. **D**: The F-actin content in chondrocytes was quantified with Image J software. All values were normalized to the F-actin of wild-type chondrocyte. Values are the mean and s.e.m. of more than three separate experiments; *, $P<0.05$, **,$P<0.05$; Scale bar, 20 μm.
doi:10.1371/journal.pone.0037163.g005

However, the present study contains a few notable limitations. Firstly this study does not show the intracellular signaling of SDF-1 in chondrocyte differentiation. **Figure 5A** showed that formation of actin stress fibers in untreated wild-type chondrocytes and chondrocytes treated with SDF-1 and TF14016 was similar, but a slight actin stress fiber formation was observed in cells treated with SDF-1 and PTX. Since PTX inactivates Gi, actin stress fiber formation with SDF-1 and PTX may also have resulted from the increase of F-actin and contraction of actomyosin through G12/13. Actin stress fiber formation for the hypertrophic transition by SDF-1 may strongly depend on Gi in addition to G12/13. This result is compatible with a previous report that RhoA/ROCK signaling, downstream of G12/13, inhibited hypertrophic differentiation [43]. SDF-1 signal transduction pathway in chondrocytes is still elusive and remains to be investigated in the future.

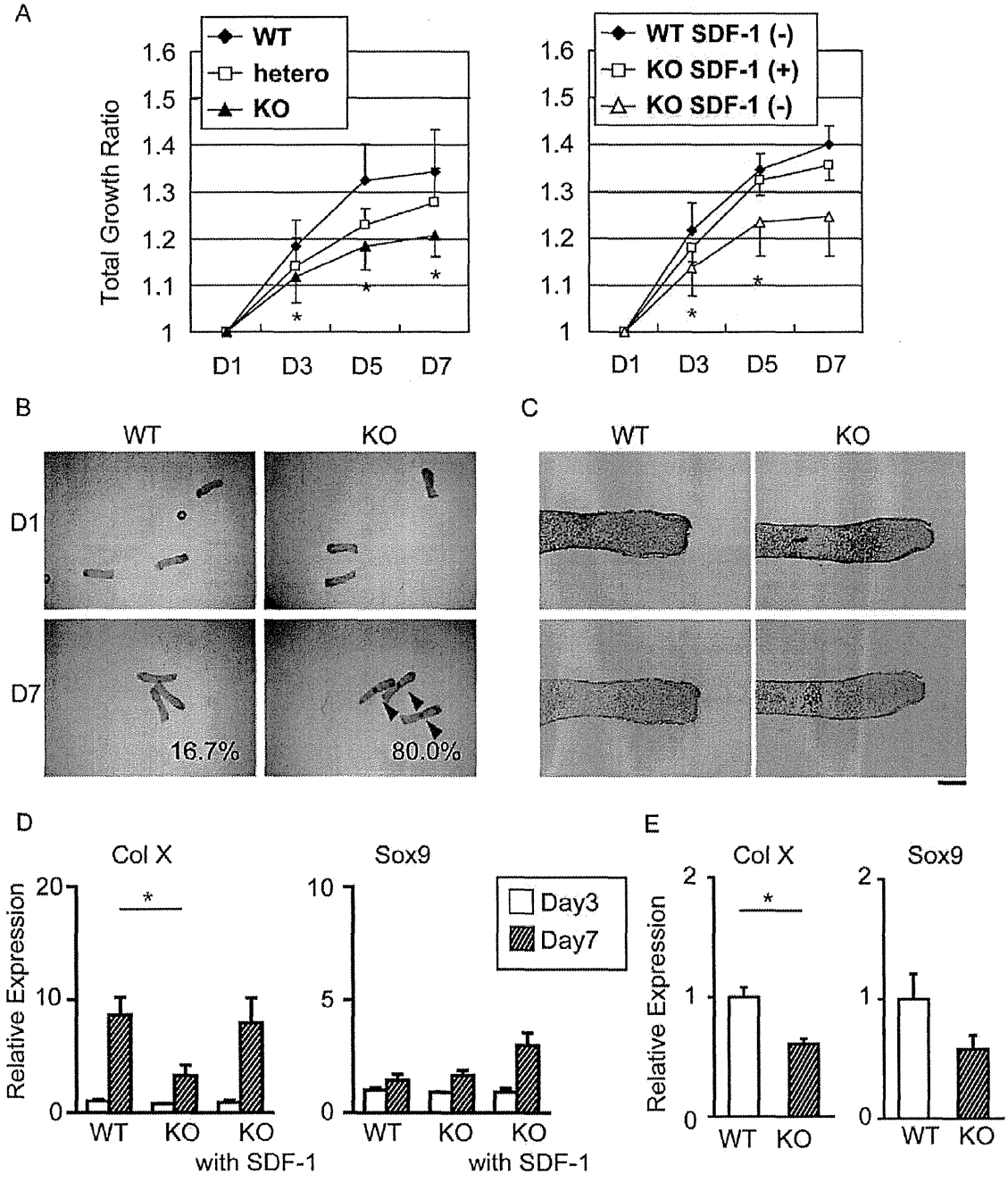

Figure 6. Lack of SDF-1 delays the growth metatarsals in organ culture. A: The metatarsal bones were harvested from SDF-$1^{-/-}$ (KO), SDF-1+/− (hetero), and wild-type (WT) mice at E15.5, cultured for 7 days, and the total length was measured at day 1, 3, 5, and 7. The length of metatarsal bones was calculated by day 1 as controls. **B**: Calcified spots (arrows) were counted in KO and WT metatarsals at day 1 and 7. **C**: Metatarsal bones were stained with hematoxylin and eosin (upper panel), or von Kossa (lower panel); Scale bar, 200 μm. **D**: The expression levels of type X collagen (Col X) and Sox9 of cultured metatarsal bones from E15.5 WT and KO mice at day 3 and 10 were quantified by real-time PCR. **E**: Primary chondrocytes isolated from WT and KO mice were cultured for 3 weeks in chondrogenic medium supplemented with insulin. The expression levels of Col X and Sox9 were quantified by real-time PCR. Values are the mean and s.e.m. of more than three independent experiments; *, $P<0.05$.
doi:10.1371/journal.pone.0037163.g006

Another relevant limitation of this study is that this study did not elucidate the association of SDF-1 signaling with other signaling molecules regulating the hypertrophic conversion of chondrocytes. RhoA/ROCK signaling, the only signaling shown to associate with actin organization during chondrogenesis, suppresses Sox9 expression [24]. Sox9 mRNA expression, however, did not show any significant difference between wild-type and SDF-$1^{-/-}$ metatarsals and primary chondrocytes in monolayer in this study

(**Figures 6D, E**). SDF-1 may regulate the hypertrophic conversion in chondrocytic differentiation and the bone growth without the involvement of Sox9, but this assumption requires further investigations.

In addition, the influence of genetic background of SDF-$1^{-/-}$ mice cannot completely be removed. As about half of SDF-$1^{-/-}$ mice start to die after E16.5 for unknown reasons, contamination of the dying embryos can affect the results. These dying embryos are easily distinguishable by their relatively small size and dark red color and we did not use these embryos for the experiments. However, there is still a possibility of the contamination. One of the solutions for this issue is the use of conditional knock-out mice. As there is no report showing mice that express Cre recombinase specifically in SDF-1-expressing prehypertrophic and/or hypertrophic chondrocytes, this issue should be pursued in the near future.

In conclusion, we investigated the role of SDF-1 in chondrocyte differentiation and revealed that SDF-1 stimulates bone growth by mediating chondrocyte hypertrophy and regulates actin polymerization.

Materials and Methods

Reagents

Recombinant mouse CXCL12/SDF-1α was purchased from R&D Systems (Minneapolis, MN). Pertussis toxin (PTX) was purchased from Sigma-Aldrich (St. Louis, MO).

Mice

All animal studies were conducted in accordance with principles by Kyoto University Committee of Animal Resources, based on International Guiding Principles for Biomedical Research Involving Animals. All procedures for this study were approved by Kyoto University Committee of Animal Resources (Permit Number: MedKyo 11260). The generation of SDF-$1^{-/-}$ mice has been previously described [45]. Heterozygotes were maintained and backcrossed more than 10 times with C57BL/6NCrSlc mice. Homozygous mutant embryos were present at the expected Mendelian ratios until E15.5, and about half of the SDF-$1^{-/-}$ embryos were dead at E18.5. The embryos that die within the uteri were slightly small in dark red color, and these were not used for the experiments.

Mouse Rib Fracture Model

Mouse rib fracture model was created using 6-week-old wild-type (C57BL/6NCrSlc) mice as previously described [46]. The mice were sacrificed at day 10 for histological analysis.

Histological Analysis and Measurement of the Ratios of Proliferating and Hypertrophic Chondrocytes

Specimens were processed to paraffin-embedded sections with a thickness of 5–7 μm, and stained with hematoxylin, eosin and alcian blue. The areas of proliferating and hypertrophic cartilages were measured by computer tracing as previously described [47]. Immunohistochemical analysis was performed to detect SDF-1 protein as previously described [22].

Visualization of Cytoskeleton in Hypertrophic Chondrocytes of the Humeri

The humeri of embryonic day 15.5 (E15.5) were isolated from wild-type embryos or crosses of SDF-$1^{+/-}$ mice. Samples were frozen in O.C.T. Compound (Sakura Finetek Japan, Tokyo, Japan). Tissues were cryosectioned at 12 μm, and briefly airdried. Sections were fixed with 4% paraformaldehyde for 20 m, followed by two washes in phosphate-buffered saline (PBS). The membranes were permeabilized with 0.5% Triton X-100/PBS solution for 20 m, and incubated in the dark for 2 h with 100 nM Rhodamine-Phalloidin (Cytoskelton, Denver, CO) and 0.01% SYBR Green I nucleic acid gel stain (Life Technologies, Carlsbad, CA). Images were taken with Nicon P-Eclipse C1 confocal microscopy equipped with objective lens 60X/1.40 oil.

Isolation and Culture of Primary Chondrocytes

Primary chondrocytes were isolated from embryonic ribs at E15.5 and cultured in Dulbecco's Modified Eagle Medium, which was regarded as post passage 0 (pp 0). When the cells became preconfluent, the cells were trypsinized and were passaged (pp 1). Cell suspensions at the cell concentration of 1×10*5 cells/ml were used for actin polymerization assay. Primary chondrocytes (pp 0) were also cultured for 3 weeks in chondrogenic medium supplemented with insulin (10 μg/ml), transferrin (5.5 μg/ml), and sodium selenite (5 ng/ml) (Sigma, St. Louis, MO) to induce chondrocyte differentiation, as previously described [48].

Actin Polymerization Assay of Primary Chondrocytes

To investigate the function of SDF-1, the cells were treated with SDF-1, TF14016, and/or PTX added to the medium for 1 m, 5 m, 10 m, 30 m, 1 h, 3 h, or 24 h. Then the cells were fixed with 4% paraformaldehyde for 10 m, and stained with 100 nM Rhodamine-Phalloidin and 0.05% 4′,6-diamidino-2-phenylindole for 30 s or 0.01% SYBR Green according to the manufacture's protocol. Images were taken Olympus IX70 laser microscopy or Nicon P-Eclipse C1 confocal microcopy, and analyzed with Image J as described before [49].

Metatarsal Organ Culture

Three central metatarsal rudiments were isolated from each hind limb of E15.5 embryos. Every three metatarsals from each limb were placed into each well of a 24-well plate containing 0.5 ml of organ culture medium as previously described [50]. The day of explant harvest was regarded as day 0 and the culture medium was replaced at day 1, and 4. SDF-1 were applied to the well containing the explants from the right hind limb, and the ones from the left hind limb were treated with culture medium alone as controls. Cultures were observed and photographed with an Olympus SZX 12 dissecting microscope at day 1, 3, 5, and 7. The cultured metatarsals were harvested at day 7 for histological procedure, and at day 3 or 7 for RNA extraction.

RNA Extraction and Quantitative Real-time PCR

Total RNA from cultured metatarsal bones were snap frozen in liquid nitrogen, homogenized, and extracted total RNA using High Pure RNA Tissue Kit (Roche Diagnostics, Penzberg, Germany). Total RNA from primary chondrocyte was extracted using High Pure RNA Isolation Kit (Roche Diagnostics). The RNA was reverse-transcribed and real-time quantitative PCR was performed using FastStart Universal SYBR Green Master (Roche Diagnostics) and ABI7500 (Life Technologies) according to the manufacturer's instructions. All of gene expression data were normalized against glyceraldehyde-3-phosphate dehydrogenase (GAPDH, forward primer, 5′- AGGTCGGTGTGAACGGATTTG, and reverse primer 5′- TGTAGACCATGTAGTTGAGGTCA). Expression patterns of Col X (forward primer, 5′-AGGCTACCTGGATCAGGCTTC, and reverse primer 5′-ACATTCTTTTCAGCCTACCTCC), and Sox9 mRNA (forward primer, 5′-GAGCCGGATCTGAAGAGGGA, and reverse

primer 5′- GCTTGACGTGTGGCTTGTTC) were also analyzed. Standard curve was generated by serially diluted plasmids containing PCR amplicon sequences. Plasmids were synthesized using pTAC-1 vector (BioDynamics Laboratory, Tokyo, Japan).

Proliferation Assay

BrdU incorporation was assessed by the cell proliferation ELISA Biotrack kit (Amersham Biosciences, Piscataway, NJ). BrdU was administrated into the mice at E15.5 2 h before the harvest. BrdU-positive cells were detected immunohistochemically as previously described [22].

Statistical Analysis

Data were analyzed with Student's t test. A p value less than 0.05 was considered statistically significant.

Supporting Information

Figure S1 BRd-U staining of embryonic humeri. A: BRd-U staining of embryonic humeri of wild-type (WT) and SDF-1$^{-/-}$ (KO) mice. Embryonic humeri of wild-type and SDF-1$^{-/-}$ mice were processed to paraffin-embedded sections and stained with Brd-U. B: The percentage of positive cells for BRd-U was calculated in WT and KO humeri.
(TIF)

Acknowledgments

We are grateful to Professor K. Tashiro (Kyoto Prefectural University of Medicine) for valuable advice on this work, and to Associate Professor Kosei Ijiri (Faculty of Medicine, Kagoshima University) for his generous help. We also thank Drs. T. Aoyama, R. Tsutsumi, K. Nishitani, and K. Yamamoto (Kyoto University Graduate School of Medicine) for their valuable technical assistance.

Author Contributions

Conceived and designed the experiments: T. Kitaori T. Nakamura HI. Performed the experiments: KM T. Kitaori ST MI T. Kasahara HS. Analyzed the data: KM T. Kitaori SO NW HY HI. Contributed reagents/materials/analysis tools: SO NW NF T. Nagasawa. Wrote the paper: KM T. Kitaori NW HI.

References

1. Karsenty G (2009) Regulation of Bone Formation. Annu Rev Cell Dev Biol. : 25, 629–48.
2. Babarina AV, Mollers U, Bittner K, Vischer P, Bruckner P (2001) Role of the subchondral vascular system in endochondral ossification: endothelial cell-derived proteinases derepress late cartilage differentiation in vitro. Matrix Biol 20: 205–213.
3. Karaplis AC, Luz A, Glowacki J, Bronson RT, Tybulewicz VL, et al. (1994) Lethal skeletal dysplasia from targeted disruption of the parathyroid hormone-related peptide gene. Genes Dev 8: 277–289.
4. Lanske B, Karaplis AC, Lee K, Luz A, Vortkamp A, et al. (1996) PTH/PTHrP receptor in early development and Indian hedgehog-regulated bone growth. Science 273: 663–666.
5. St-Jacques B, Hammerschmidt M, McMahon AP (1999) Indian hedgehog signaling regulates proliferation and differentiation of chondrocytes and is essential for bone formation. Genes Dev 13: 2072–2086.
6. Hartmann C, Tabin CJ (2000) Dual roles of Wnt signaling during chondrogenesis in the chicken limb. Development 127: 3141–3159.
7. Akiyama H, Lyons JP, Mori-Akiyama Y, Yang X, Zhang R, et al. (2004) Interactions between Sox9 and beta-catenin control chondrocyte differentiation. Genes Dev 18: 1072–1087.
8. Murakami S, Balmes G, McKinney S, Zhang Z, Givol D, et al. (2004) Constitutive activation of MEK1 in chondrocytes causes Stat1-independent achondroplasia-like dwarfism and rescues the Fgfr3-deficient mouse phenotype. Genes Dev 18: 290–305.
9. Tashiro K, Tada H, Heilker R, Shirozu M, Nakano T, et al. (1993) Signal sequence trap: a cloning strategy for secreted proteins and type I membrane proteins. Science 261: 600–603.
10. Nagasawa T, Kikutani H, Kishimoto T (1994) Molecular cloning and structure of a pre-B-cell growth-stimulating factor. Proc Natl Acad Sci U S A 91: 2305–2309.
11. Bleul CC, Farzan M, Choe H, Parolin C, Clark-Lewis I, et al. (1996) The lymphocyte chemoattractant SDF-1 is a ligand for LESTR/fusin and blocks HIV-1 entry. Nature 382: 829–833.
12. Hartmann TN, Grabovsky V, Pasvolsky R, Shulman Z, Buss EC, et al. (2008) A crosstalk between intracellular CXCR7 and CXCR4 involved in rapid CXCL12-triggered integrin activation but not in chemokine-triggered motility of human T lymphocytes and CD34+ cells. J Leukoc Biol 84: 1130–1140.
13. Levoye A, Balabanian K, Baleux F, Bachelerie F, Lagane B (2009) CXCR7 heterodimerizes with CXCR4 and regulates CXCL12-mediated G protein signaling. Blood 113: 6085–6093.
14. Wynn RF, Hart CA, Corradi-Perini C, O'Neill L, Evans CA, et al. (2004) A small proportion of mesenchymal stem cells strongly expresses functionally active CXCR4 receptor capable of promoting migration to bone marrow. Blood 104: 2643–2645.
15. Dar A, Goichberg P, Shinder V, Kalinkovich A, Kollet O, et al. (2005) Chemokine receptor CXCR4-dependent internalization and resecretion of functional chemokine SDF-1 by bone marrow endothelial and stromal cells. Nat Immunol 6: 1038–1046.
16. Kucia M, Ratajczak J, Reca R, Janowska-Wieczorek A, Ratajczak MZ (2004) Tissue-specific muscle, neural and liver stem/progenitor cells reside in the bone marrow, respond to an SDF-1 gradient and are mobilized into peripheral blood during stress and tissue injury. Blood Cells Mol Dis 32: 52–57.
17. Abbott JD, Huang Y, Liu D, Hickey R, Krause DS, et al. (2004) Stromal cell-derived factor-1alpha plays a critical role in stem cell recruitment to the heart after myocardial infarction but is not sufficient to induce homing in the absence of injury. Circulation 110: 3300–3305.
18. Ma J, Ge J, Zhang S, Sun A, Shen J, et al. (2005) Time course of myocardial stromal cell-derived factor 1 expression and beneficial effects of intravenously administered bone marrow stem cells in rats with experimental myocardial infarction. Basic Res Cardiol 100: 217–223.
19. Ji JF, He BP, Dheen ST, Tay SS (2004) Interactions of chemokines and chemokine receptors mediate the migration of mesenchymal stem cells to the impaired site in the brain after hypoglossal nerve injury. Stem Cells 22: 415–427.
20. Togel F, Isaac J, Hu Z, Weiss K, Westenfelder C (2005) Renal SDF-1 signals mobilization and homing of CXCR4-positive cells to the kidney after ischemic injury. Kidney Int 67: 1772–1784.
21. Avniel S, Arik Z, Maly A, Sagie A, Basst HB, et al. (2006) Involvement of the CXCL12/CXCR4 pathway in the recovery of skin following burns. J Invest Dermatol 126: 468–476.
22. Kitaori T, Ito H, Schwarz EM, Tsutsumi R, Yoshitomi H, et al. (2009) Stromal cell-derived factor 1/CXCR4 signaling is critical for the recruitment of mesenchymal stem cells to the fracture site during skeletal repair in a mouse model. Arthritis Rheum 60: 813–823.
23. von der Mark K, von der Mark H (1977) Immunological and biochemical studies of collagen type transition during in vitro chrondrogenesis of chick limb mesodermal cells. J Cell Biol 73: 736–747.
24. Woods A, Wang G, Beier F (2005) RhoA/ROCK signaling regulates Sox9 expression and actin organization during chondrogenesis. J Biol Chem 280: 11626–11634.
25. Woods A, Beier F (2006) RhoA/ROCK signaling regulates chondrogenesis in a context-dependent manner. J Biol Chem 281: 13134–13140.
26. Kumar D, Lassar AB (2009) The transcriptional activity of Sox9 in chondrocytes is regulated by RhoA signaling and actin polymerization. Mol Cell Biol 29: 4262–4273.
27. Alsayed Y, Ngo H, Runnels J, Leleu X, Singha UK, et al. (2007) Mechanisms of regulation of CXCR4/SDF-1 (CXCL12)-dependent migration and homing in multiple myeloma. Blood 109: 2708–2717.
28. Azab AK, Azab F, Blotta S, Pitsillides CM, Thompson B, et al. (2009) RhoA and Rac1 GTPases play major and differential roles in stromal cell-derived factor-1-induced cell adhesion and chemotaxis in multiple myeloma. Blood 114: 619–629.
29. Tamamura H, Hiramatsu K, Mizumoto M, Ueda S, Kusano S, et al. (2003) Enhancement of the T140-based pharmacophores leads to the development of more potent and bio-stable CXCR4 antagonists. Org Biomol Chem 1: 3663–3669.
30. Raz E, Mahabaleshwar H (2009) Chemokine signaling in embryonic cell migration: a fisheye view. Development 136: 1223–1229.
31. Tachibana K, Hirota S, Iizasa H, Yoshida H, Kawabata K, et al. (1998) The chemokine receptor CXCR4 is essential for vascularization of the gastrointestinal tract. Nature 393: 591–594.
32. Zou YR, Kottmann AH, Kuroda M, Taniuchi I, Littman DR (1998) Function of the chemokine receptor CXCR4 in haematopoiesis and in cerebellar development. Nature 393: 595–599.
33. Grassi F, Cristino S, Toneguzzi S, Piacentini A, Facchini A, et al. (2004) CXCL12 chemokine up-regulates bone resorption and MMP-9 release by

human osteoclasts: CXCL12 levels are increased in synovial and bone tissue of rheumatoid arthritis patients. J Cell Physiol 199: 244–251.
34. Sun YX, Schneider A, Jung Y, Wang J, Dai J, et al. (2005) Skeletal localization and neutralization of the SDF-1(CXCL12)/CXCR4 axis blocks prostate cancer metastasis and growth in osseous sites in vivo. J Bone Miner Res 20: 318–329.
35. Jung Y, Wang J, Schneider A, Sun YX, Koh-Paige AJ, et al. (2006) Regulation of SDF-1 (CXCL12) production by osteoblasts; a possible mechanism for stem cell homing. Bone 38: 497–508.
36. Wei L, Kanbe K, Lee M, Wei X, Pei M, et al. (2010) Stimulation of chondrocyte hypertrophy by chemokine stromal cell-derived factor 1 in the chondro-osseous junction during endochondral bone formation. Dev Biol 341: 236–245.
37. Doitsidou M, Reichman-Fried M, Stebler J, Koprunner M, Dorries J, et al. (2002) Guidance of primordial germ cell migration by the chemokine SDF-1. Cell 111: 647–659.
38. Vicente-Manzanares M, Viton M, Sanchez-Madrid F (2004) Measurement of the levels of polymerized actin (F-actin) in chemokine-stimulated lymphocytes and GFP-coupled cDNA transfected lymphoid cells by flow cytometry. Methods Mol Biol 239: 53–68.
39. van Buul JD, Voermans C, van Gelderen J, Anthony EC, van der Schoot CE, et al. (2003) Leukocyte-endothelium interaction promotes SDF-1-dependent polarization of CXCR4. J Biol Chem 278: 30302–30310.
40. Vicente-Manzanares M, Cabrero JR, Rey M, Perez-Martinez M, Ursa A, et al. (2002) A role for the Rho-p160 Rho coiled-coil kinase axis in the chemokine stromal cell-derived factor-1alpha-induced lymphocyte actomyosin and microtubular organization and chemotaxis. J Immunol 168: 400–410.
41. Watanabe N (2010) Inside view of cell locomotion through single-molecule: fast F-/G-actin cycle and G-actin regulation of polymer restoration. Proc Jpn Acad Ser B Phys Biol Sci 86: 62–83.
42. Saltel F, Chabadel A, Bonnelye E, Jurdic P (2008) Actin cytoskeletal organisation in osteoclasts: a model to decipher transmigration and matrix degradation. Eur J Cell Biol 87: 459–468.
43. Wang G, Woods A, Sabari S, Pagnotta L, Stanton LA, et al. (2004) RhoA/ROCK signaling suppresses hypertrophic chondrocyte differentiation. J Biol Chem 279: 13205–13214.
44. Kronenberg HM (2003) Developmental regulation of the growth plate. Nature 423: 332–336.
45. Nagasawa T, Hirota S, Tachibana K, Takakura N, Nishikawa S, et al. (1996) Defects of B-cell lymphopoiesis and bone-marrow myelopoiesis in mice lacking the CXC chemokine PBSF/SDF-1. Nature 382: 635–638.
46. Ito H, Akiyama H, Shigeno C, Iyama K, Matsuoka H, et al. (1999) Hedgehog signaling molecules in bone marrow cells at the initial stage of fracture repair. Biochem Biophys Res Commun 262: 443–451.
47. Ito H, Koefoed M, Tiyapatanaputi P, Gromov K, Goater JJ, et al. (2005) Remodeling of cortical bone allografts mediated by adherent rAAV-RANKL and VEGF gene therapy. Nat Med 11: 291–297.
48. Fukai A, Kawamura N, Saito T, Oshima Y, Ikeda T, et al. (2010) Akt1 in murine chondrocytes controls cartilage calcification during endochondral ossification under physiologic and pathologic conditions. Arthritis Rheum 62: 826–836.
49. Stein CA, Wu S, Voskresenskiy AM, Zhou JF, Shin J, et al. (2009) G3139, an anti-Bcl-2 antisense oligomer that binds heparin-binding growth factors and collagen I, alters in vitro endothelial cell growth and tubular morphogenesis. Clin Cancer Res 15: 2797–2807.
50. Alvarez J, Sohn P, Zeng X, Doetschman T, Robbins DJ, et al. (2002) TGFbeta2 mediates the effects of hedgehog on hypertrophic differentiation and PTHrP expression. Development 129: 1913–1924.